

# 1 **Future tropospheric ozone budget and distribution over** 2 **East Asia under a Net Zero scenario**

3 Xuewei Hou<sup>1,4</sup>, Oliver Wild<sup>2</sup>, Bin Zhu<sup>1</sup>, James Lee<sup>3,5</sup>

4 <sup>1</sup>Collaborative Innovation Center on Forecast and Evaluation of Meteorological Disasters, Key  
5 Laboratory of Meteorological Disaster, Ministry of Education (KLME), School of Atmospheric  
6 Physics, Nanjing University of Information Science and Technology, Nanjing, China

7 <sup>2</sup>Lancaster Environment Centre, Lancaster University, Lancaster, UK

8 <sup>3</sup>Department of Chemistry, University of York, York, UK

9 <sup>4</sup>Key Laboratory of Atmospheric Chemistry, China Meteorological Administration, Beijing  
10 (LAC/CMA), China

11 <sup>5</sup>National Centre for Atmospheric Science, York, UK

12 *Correspondence to:* Xuewei Hou (houxw@nuist.edu.cn)

13 **Abstract:** Under future net zero emission policies, reductions in emissions of ozone (O<sub>3</sub>) precursors are  
14 expected to alter the temporal and spatial distribution of tropospheric O<sub>3</sub>. In this study, we quantify  
15 changes in the tropospheric O<sub>3</sub> budget, spatiotemporal distribution of surface O<sub>3</sub> in East Asia and the  
16 contributions from regional emissions, intercontinental transport and climate change between the present  
17 day and 2060 under a net zero scenario, using the NCAR Community Earth System Model (CESM) with  
18 online tagging of O<sub>3</sub> and its precursors. The results reveal that the global tropospheric O<sub>3</sub> burden is likely  
19 to decrease by more than 20%, from 316 Tg in present day to 247 Tg in 2060, under a net zero scenario.  
20 The burden of stratospheric O<sub>3</sub> in the troposphere is expected to increase from 69 to 77 Tg. The mean  
21 lifetime of tropospheric O<sub>3</sub> increases by 2 days, ~10%. Changes in climate under a net zero pathway are  
22 relatively small, and only lead to small increases in tropospheric O<sub>3</sub>. Over East China, surface O<sub>3</sub>  
23 increases in winter, due to the weakened titration of O<sub>3</sub> by NO associated with reduced anthropogenic  
24 NO emissions, and to enhanced stratospheric input. In summer, surface O<sub>3</sub> decreases by more than 30  
25 ppbv, and peak concentrations shift from July to May. Local contributions from anthropogenic emissions  
26 to surface O<sub>3</sub> over East Asia are highest in summer, but drop substantially, from 30% to 14%, under a  
27 net zero scenario. The contribution of biogenic NO sources is enhanced, and forms the dominant  
28 contributor to future surface O<sub>3</sub>, especially in summer, ~40%. This enhanced contribution is mainly due  
29 to the increased O<sub>3</sub> production efficiency under lower anthropogenic precursor emissions. Over Eastern  
30 China, local anthropogenic contributions decrease from 50% to 30%. The decreases in surface O<sub>3</sub> are  
31 strongly beneficial and are more than sufficient to counteract the increases in surface O<sub>3</sub> observed in  
32 China over recent years. This study thus highlights the important co-benefits of net zero policies that  
33 target climate change in addressing surface O<sub>3</sub> pollution over East Asia.

34 **Keywords:** Tropospheric O<sub>3</sub>; SSP1-1.9 pathway; net zero; O<sub>3</sub> budgets; stratospheric contribution

## 35 **1 Introduction**

36 Although ozone (O<sub>3</sub>) occurs naturally in small quantities in the lower troposphere, unhealthy levels of  
37 tropospheric O<sub>3</sub> are created when high levels of anthropogenic pollutants, such as nitrogen oxides (NO<sub>x</sub>),  
38 and volatile organic compounds (VOCs) are oxidized in the presence of solar radiation. This excess O<sub>3</sub>  
39 acts as a pollutant and greenhouse gas, contributing to harmful smog that damages human health and  
40 ecosystems (Jerrett et al., 2009; Malley et al., 2017; Emberson, 2020) and contributing to higher  
41 tropospheric temperatures (Myhre et al., 2013; Stevenson et al., 2013). The relatively short lifetime of  
42 O<sub>3</sub> in the troposphere (~3 weeks, Young et al., 2013) means that it is classified as a Near Term Climate  
43 Forcer (NTCF), having an important influence on climate over shorter timescales than the long-lived  
44 greenhouse gases such as CO<sub>2</sub>. Tropospheric O<sub>3</sub> is also an oxidant and a precursor for the hydroxyl (OH)  
45 radical (Griffiths et al., 2021). OH (and by implication O<sub>3</sub>) controls the lifetime of methane (Voulgarakis  
46 et al., 2013), the second most important anthropogenic greenhouse gas after carbon dioxide (Myhre et  
47 al., 2013). Oxidant levels mediate the formation of secondary aerosols such as sulfate and nitrate and  
48 play a major role in the aerosol budget and burden with important consequences for radiative forcing  
49 (Shindell et al., 2009; Karset et al., 2018). Understanding how tropospheric O<sub>3</sub> changes is important for  
50 both future air quality and climate (Turnock et al., 2019).

51 A multi-model assessment of future changes in tropospheric O<sub>3</sub> was made in the Atmospheric Chemistry  
52 and Climate Model Intercomparison Project (ACCMIP), using future changes in climate and O<sub>3</sub> precursor  
53 emissions from the Representative Concentration Pathways (RCPs) (Lamarque et al., 2013). The models  
54 participating in ACCMIP projected changes in global annual mean surface O<sub>3</sub> concentrations between  
55 2000 and 2030 of ±1.5 ppbv under the different RCPs (Young et al., 2013). More recent single model  
56 estimates by O'Connor et al. (2014) and Kim et al. (2015) predict surface O<sub>3</sub> responses across the different  
57 RCPs of between -4.0 and +2.0 ppbv by 2050 relative to 2000. The global annual mean tropospheric O<sub>3</sub>  
58 burden was projected to change by between -18% and +20% from 2000 to 2100 under the different RCPs  
59 (Cionni et al., 2011; Kawase et al., 2011; O'Connor et al., 2014; Young et al., 2013). Whether  
60 tropospheric O<sub>3</sub> increases or decreases in future is dependent on the climate mitigation measures and air  
61 pollution policies that are implemented. In preparation for the sixth Coupled Model Intercomparison  
62 Project (CMIP6), a new set of future pathways was created. Five different socio-economic pathways  
63 (SSPs) were developed with centennial trends based on different combinations of social, economic and  
64 environmental developments (O'Neill et al., 2014). Different levels of emissions mitigation were  
65 included within each SSP to meet particular climate and air pollution targets (Rao et al., 2017; Riahi et  
66 al., 2017). They incorporate stronger links between socio-economic development patterns and climate  
67 change risks than previous assessments and provide better hypothetical scenarios for future projections.  
68 The five most widely-used scenarios are SSP1-1.9, SSP1-2.6, SSP2-4.5, SSP3-7.0, and SSP5-8.5, where  
69 SSP1-SSP5 represent differing socio-economic pathways and the suffix 1.9-8.5 indicates the total  
70 radiative forcing (W/m<sup>2</sup>) at the end of the 21st century compared with that before the Industrial  
71 Revolution. These pathways provide a good foundation for assessment of air quality, radiative forcing,  
72 ecological environmental effects and human health effects in the future. Many studies have focused on

73 the pessimistic SSP3-7.0 scenario reflecting regional rivalry, and Griffiths et al. (2021) demonstrates that  
74 the tropospheric O<sub>3</sub> burden increases from 356 ± 31 Tg in present day to 416 ± 35 Tg in 2100 under this  
75 pathway. Liu et al. (2022) shows that the tropospheric O<sub>3</sub> burden increases by 4 % between 2010 and  
76 2050 under SSP3-7.0. Based on multi-model simulations conducted for the Aerosol and Chemistry  
77 Model Intercomparison Project (AerChemMIP), Allen et al. (2020) and Zanis et al. (2022) reveal a global  
78 surface O<sub>3</sub> decrease in future along the SSP3-7.0 scenario, due to enhanced ozone destruction from higher  
79 water vapor abundances under a warmer climate. The sustainability-focused SSP1-1.9 pathway is the  
80 scenario mostly closely aligned with recent pledges aiming at net zero greenhouse gas emissions, limiting  
81 warming to 1.5°C by 2100, but the impacts of this pathway on tropospheric O<sub>3</sub> are less well studied and  
82 remain unclear.

83 In East Asia, surface O<sub>3</sub> has increased rapidly since 2000 (Lu et al., 2020), and is expected to increase  
84 by another ~10 ppbv by 2050 following the IPCC A1B (Wang et al., 2013), RCP6.0 (Zhu and Liao, 2016)  
85 and RCP4.5 (Hong et al., 2019) scenarios. In September 2020, China committed to achieve carbon  
86 neutrality by 2060, following the commitments of many developed countries to achieve net zero  
87 emissions by 2050. The effect of these strong mitigation measures on surface O<sub>3</sub> has not been explored  
88 thoroughly, but the proposed emission pathway to net zero loosely aligns with the SSP1-1.9 pathway.  
89 Turnock et al (2019) showed large reductions of more than 8 ppbv in surface O<sub>3</sub> over East Asia by 2050  
90 along this pathway due to large reductions in precursor emissions and CH<sub>4</sub>. The study also shows that  
91 any benefits to surface O<sub>3</sub> from reducing local emission sources over East Asia could be offset by  
92 intercontinental transport of O<sub>3</sub> formed from sources remote to the region and from global CH<sub>4</sub> sources.  
93 This analysis used an O<sub>3</sub> parameterization to rapidly assess changes in O<sub>3</sub> and source attribution (Wild  
94 et al., 2012; Turnock et al., 2018), which did not account for changes in climate, stratosphere-to-  
95 troposphere exchange, or chemical regime. Other recent assessments exploring the implications of  
96 carbon neutrality in China have suggested that O<sub>3</sub> concentrations may decline to 63-94 µg m<sup>-3</sup> by 2060  
97 (Shi et al., 2021; Wang and Liao, 2022; Xu et al., 2022). The differences between these results have been  
98 attributed to the emission and climate scenarios used. Wang and Liao (2022) also found that the annual  
99 mean contribution of Southeast Asia to surface MDA8 O<sub>3</sub> in China is 3-19 µg m<sup>-3</sup>, about 2-10 ppbv, and  
100 this contribution is reduced in future along the SSP1-1.9 pathway.

101 While previous studies have quantified possible changes in surface O<sub>3</sub> under carbon neutrality, the wider  
102 impact on the global tropospheric O<sub>3</sub> budget and the changing contributions of different sources remain  
103 unclear. In this study, we quantify the changes in surface O<sub>3</sub> over East Asia, and especially over Eastern  
104 China which currently has high anthropogenic emissions, and the contribution of different sources based  
105 on emissions and climate change along the SSP1-1.9 pathway, using the NCAR Community Earth  
106 System Model (CESM) with online tagging of O<sub>3</sub> and its precursors. We present a self-consistent  
107 assessment of the changes in surface O<sub>3</sub> associated with changes in emissions and climate, along with  
108 the first attribution of these changes. The paper is organized as follows. Section 2 describes the model  
109 configurations, experimental settings, O<sub>3</sub> tagging method, and evaluation datasets. In section 3, O<sub>3</sub> and  
110 NO<sub>x</sub> in present day simulations are evaluated against observations. In section 4, changes in tropospheric  
111 O<sub>3</sub> under the net zero scenario are presented. In section 5, the contribution of O<sub>3</sub> chemistry and

112 intercontinental transport are discussed under present day and future conditions. We close with a  
113 summary in section 6.

## 114 **2 Materials and methods**

### 115 **2.1 Model configurations and experiments**

116 The NCAR CESM is a coupled climate model incorporating components for simulating the Earth's  
117 atmosphere, ocean, land, land-ice, and sea-ice (e.g., Neale et al., 2013; Lamarque et al., 2012; Tilmes et  
118 al., 2015; Danabasoglu et al., 2020), allowing fundamental research into the Earth's past, present, and  
119 future climate states. CESM showed excellent performance in CMIP6 (Eyring et al., 2016; Fan et al.,  
120 2020; Yang et al., 2021). The experiments here use CESM version 1.2.2  
121 (<https://www.cesm.ucar.edu/models/cesm1.2/>) and the latest version 2.2.0  
122 (<https://www.cesm.ucar.edu/models/cesm2/>) to reproduce present-day O<sub>3</sub> mixing ratios and to predict O<sub>3</sub>  
123 responses to emissions and climate in the future along the SSP1-1.9 pathway. All model simulations are  
124 performed with prescribed sea surface temperatures and sea ice distribution data for climatological  
125 conditions in present day and future net zero, since we focus on the atmospheric component. Dry  
126 deposition of gases and aerosols are implemented in the Community Land Model (Oleson, 2010) as  
127 described in Lamarque et al. (2012).

128 Atmospheric chemistry of gas phase and aerosol species in the global Community Atmosphere Model  
129 (CAM version 4, Neale et al., 2013; CAM version 6, Danabasoglu et al., 2020), the atmospheric  
130 component of CESM, is represented by CAM-chem. CAM-chem provides the flexibility of using the  
131 same code to perform climate simulations (online) and simulations with specified meteorological fields  
132 (offline). The chemical mechanism is based on the Model for Ozone and Related chemical Tracers  
133 (MOZART), version 4 mechanism for the troposphere (Emmons et al., 2010), extended for stratospheric  
134 chemistry (Kinnison et al., 2007), with further updates as described in Lamarque et al. (2012), including  
135 additional reaction rate updates following JPL-2010 recommendations (Sander et al., 2011).

136 In this paper, offline simulations are used to investigate the effect of emission changes on tropospheric  
137 O<sub>3</sub> under fixed meteorological parameters, while online simulations are used for the effects of emission  
138 and climate changes with two-way feedback of atmospheric components and meteorological parameters.  
139 Two different versions of CESM are used in this study due to the application of online tagging of O<sub>3</sub> and  
140 its precursors, which is only fully tested and evaluated in CESM1. The use of a similar chemical  
141 mechanism (MOZART) in different model versions may reduce the uncertainties in the simulation results.  
142 All simulations discussed in this paper are performed at a horizontal resolution of 1.9° (latitude) and 2.5°  
143 (longitude). The model has 26 vertical levels in the online configuration and 56 levels in the offline  
144 configuration using specified meteorological fields; in all these cases, the model extends to  
145 approximately 4 hPa (≈40 km). Offline simulations were driven by Modern Era Retrospective analysis  
146 for Research and Applications, version 2 (MERRA2) meteorology (Rienecker et al., 2011). Simulations  
147 using present-day emissions (2015) are labelled PD, while those using future net zero emissions (2060)  
148 are labelled NZ, and these are prefixed with online or offline depending on whether the model is run

149 online or driven by MERRA2 meteorology. To ensure the stability of the response to climate change, the  
 150 future online simulations are run for 15 years, with the first ten years as spin-up. The CH<sub>4</sub> concentrations  
 151 are prescribed following the SSP1-1.9 pathway using a fixed lower boundary condition. A summary of  
 152 the simulations is provided in Table 1.

153

Table 1 Experimental settings

Case-name	Climate Change and Emissions		Emissions		
	online-PD	online-NZ	offline-PD	offline-NZ	
Model	CESM1.2.2	CESM1.2.2	CESM2.2.0	CESM2.2.0	
Component	FMOZ	FMOZ	FCSD	FCSD	
Physics	CAM4	CAM4	CAM6	CAM6	
Chemical mechanism	tropospheric chemistry with bulk aerosols, MOZART-4		troposphere/stratosphere chemistry with simplified VBS-SOA, MOZART-TS1		
Dynamics	Free-running	Free-running	Merra2 Nudging	Merra2 Nudging	
Spin-up	2012-2014	2050-2059	2014	2014	
Analyzed Year	2015-2016	2060-2064	2015	2015	
Resolution	1.9°×2.5° with 26 levels	1.9°×2.5° with 26 levels	1.9°×2.5° with 56 levels	1.9°×2.5° with 56 levels	
	in China	2015- DPEC	2060-DPEC	2015-DPEC	2060-DPEC
Emission	Outside China	2015-SSP119	2060-SSP119	2015-SSP119	2060-SSP119
CH <sub>4</sub>		2015-SSP119	2060-SSP119	2015-SSP119	2060-SSP119
Tagging O <sub>3</sub> sources	TOAST		O <sub>3</sub> S		

154

## 155 2.2 Emissions

156 For this analysis, we use estimates of global future anthropogenic and biomass burning emissions and  
 157 future abundances of greenhouse gases and aerosols provided by the SSP1-1.9 pathway ([https://esgf-  
 158 node.llnl.gov/projects/input4mips/](https://esgf-node.llnl.gov/projects/input4mips/)) along with more recent estimates for China using the Ambitious-  
 159 pollution-Neutral-goals scenario from the Dynamic Projection model for Emissions in China (DPEC,  
 160 <http://meicmodel.org/>). The SSP1-1.9 pathway results in a climate radiative forcing of 1.9 W m<sup>-2</sup> by 2100  
 161 under the sustainable development path. The SSP1-1.9 pathway is a strong pollution control scenario and  
 162 is the only route to limit the global average temperature increase since the preindustrial period to 1.5°C  
 163 by 2100 (O'Neill et al., 2014; Rao et al., 2017; Riahi et al., 2017). The emissions inventory includes  
 164 monthly O<sub>3</sub> precursors, aerosols, and their precursors (NO<sub>x</sub>, CO, non-methane volatile organic (VOCs),  
 165 sulfur dioxide (SO<sub>2</sub>), ammonia (NH<sub>3</sub>), black carbon (BC), organic carbon (OC), dimethyl sulphide  
 166 (DMS)), and concentrations of greenhouse gases, such as CH<sub>4</sub>. Biogenic emissions of VOCs are

167 calculated online in CESM using the Model of Emissions of Gases and Aerosols from Nature model  
 168 (MEGAN; Guenther et al., 2006; 2012). We use emissions for the years 2015 and 2060. Over China, the  
 169 anthropogenic emissions are replaced by the Ambitious-pollution-Neutral- goals scenario from DPEC  
 170 (Tong et al., 2020; Cheng et al., 2021). This considers a scenario in which China achieves carbon  
 171 neutrality by 2060. The DPEC anthropogenic emissions are based on SSP scenarios and MEIC, but give  
 172 anthropogenic emissions at higher resolution in China which more accurately characterize China's  
 173 emission sources and reflect recent rapid changes in emissions. The total anthropogenic NO emission in  
 174 China in the Ambitious-pollution-Neutral- goals scenario from DPEC is 1.1 Tg yr<sup>-1</sup> lower in present day  
 175 than in SSP1-1.9 and 1.5 Tg yr<sup>-1</sup> lower in 2060, but in most regions of Eastern China it is slightly higher.  
 176 The combined emissions distribution for NO<sub>x</sub> and its changes in future are shown in Figure S1. The total  
 177 annual mean surface emissions of key pollutants from anthropogenic (ANT), biomass burning (BB) and  
 178 biogenic (BIO) sources for the present day (2015) and future net zero (2060) over the globe and in East  
 179 Asia are listed in Table 2.

180 The global anthropogenic emissions of all O<sub>3</sub> precursors are significantly reduced in the net zero scenario.  
 181 Due to strict control policies on pollutants emissions and changes in technology and behavior, global  
 182 anthropogenic NO emissions decrease from 87 Tg yr<sup>-1</sup> in present day to 19 Tg yr<sup>-1</sup> in 2060, and total  
 183 anthropogenic VOCs emissions decrease from 125 Tg yr<sup>-1</sup> to 28 Tg yr<sup>-1</sup>. Biomass burning emissions also  
 184 decrease slightly. Natural NO soil emission, VOCs biogenic emission, and CO ocean emission are  
 185 assumed not to change in this study as changes in land use are relatively small. Anthropogenic emissions  
 186 over East Asia account for more than 35% of the global total, with biomass combustion emissions  
 187 accounting for a smaller proportion, ~10%, and natural emissions of NO, VOCs and CO accounting for  
 188 ~20%. The decrease of anthropogenic emissions over East Asia (about 80% for NO) is greater than the  
 189 global average, >70%, which may be due to the high present-day emissions over the region, especially  
 190 in Eastern China. The global CH<sub>4</sub> concentration decreases from the current 1831 ppbv to 1312 ppbv, due  
 191 to the lower global CH<sub>4</sub> emissions under net zero.

192 Table 2 Annual mean time-varying surface emissions of NO<sub>x</sub>, VOCs, and CO from anthropogenic  
 193 (ANT), biomass burning (BB) and biogenic (BIO) emissions for the present day (2015) and future  
 194 (2060, net zero) in East Asia and over the globe. Annual mean surface CH<sub>4</sub> mixing ratios (ppbv) are  
 195 also shown.

Emission (Tg yr <sup>-1</sup> )		Globe		East Asia	
		Present Day	Net Zero	Present Day	Net Zero
NO	ANT	87.5	19.1	36.9	7.5
	BB	8.9	7.5	0.7	0.5
	Soil	10.6	10.6	2.3	2.3
	Total	106.9	37.2	39.8	10.2
VOCs	ANT	125.0	27.5	42.9	11.0

	BB	66.6	50.2	6.3	4.0
	BIO	868.5	868.5	111.0	111.0
	Total	1060.1	946.2	160.3	126.0
CO	ANT	559.8	151.7	266.9	72.7
	BB	325.5	248.2	30.2	18.9
	Ocean	20.0	20.0	1.3	1.3
	Total	905.2	419.9	298.4	92.9
CH <sub>4</sub> (ppbv)		1830.5	1312.2	1860.8	1337.3

196

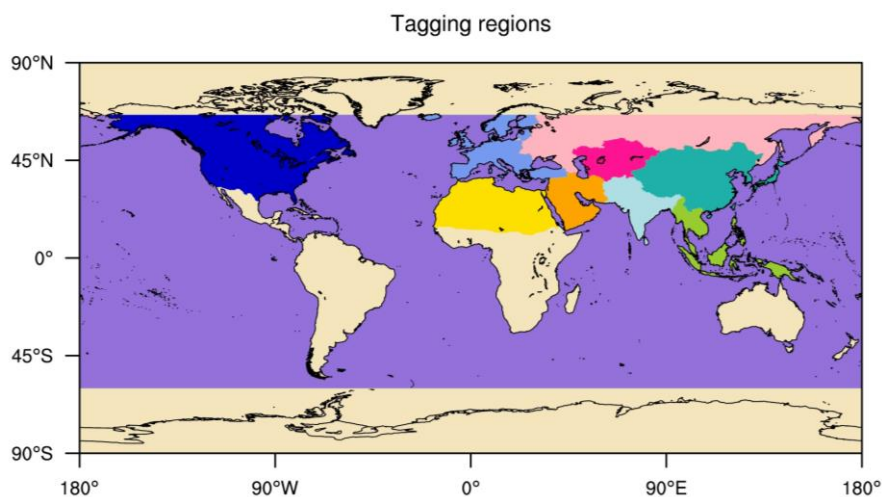
### 197 2.3 Tagging of ozone

198 In this study, we use the Tropospheric Ozone Attribution of Sources with Tagging (TOAST) ozone  
 199 methodology in CESM1.2.2 previously described by Butler et al. (2018, 2020) to perform separate source  
 200 attributions of ground-level O<sub>3</sub> to NO<sub>x</sub>. The parameterizations based on the work of Butler et al. (2018,  
 201 2020) include tagging the biogenic, biomass burning and anthropogenic emissions of NO<sub>x</sub> or VOCs by  
 202 their geographical source regions. This tagging methodology allows us to examine the seasonal cycle of  
 203 the surface O<sub>3</sub> attribution in receptor regions using those defined in the Hemispheric Transport of Air  
 204 Pollutants Phase 2 (HTAP2, Janssens-Maenhout et al., 2015; Koffi et al., 2016). We consider 16 sources,  
 205 including 11 geographical source regions for anthropogenic NO<sub>x</sub> emission, shown in Table 3 and Figure  
 206 1, NO<sub>x</sub> emissions from biogenic sources (BIO), biomass burning (BB), aircraft (AIR) and lightning  
 207 (LIG), and O<sub>3</sub> originating in the stratosphere (STR).

208 Table 3 Source sector tagging of anthropogenic NO<sub>x</sub> emissions by geographical source region, NO<sub>x</sub>  
 209 emissions from biogenic burning, soil emission, aircraft, and lightning, and the contribution of  
 210 stratospheric O<sub>3</sub> input.

ID	Geographical region, NO <sub>x</sub>	ID	Geographical region, NO <sub>x</sub>	ID	Source
OCN	Oceans	NAF	Northern Africa	BIO	Biogenic NO <sub>x</sub>
NAM	N. America	MDE	Middle East	BB	Bioburn NO <sub>x</sub>
EUR	Europe	CAS	Central Asia	AIR	Aircraft NO <sub>x</sub>
SAS	South Asia	SEA	South East Asia	LIG	Lightning NO <sub>x</sub>
EAS	East Asia	RBU	Russia, Belarus, Ukraine	STR	Stratospheric O <sub>3</sub>
RST	Rest of World				

211



212

213 Figure 1 Geographical source regions for tagging anthropogenic NO<sub>x</sub> emissions in this study as defined  
 214 in HTAP Phase 2.

215 **2.4 Measurement Data**

216 To evaluate tropospheric column O<sub>3</sub> in the model simulations, we use a present-day satellite dataset of  
 217 tropospheric column O<sub>3</sub>, which was derived by combining retrievals from the Aura Ozone Monitoring  
 218 Instrument (OMI) and Microwave Limb Sounder (MLS) observations ([https://acd-  
 219 ext.gsfc.nasa.gov/Data\\_services/cloud\\_slice/](https://acd-ext.gsfc.nasa.gov/Data_services/cloud_slice/)). More details about the generation of this dataset are  
 220 provided by Ziemke et al., (2011). The dataset resolution used in this study is 1° (Latitude) ×1.25°  
 221 (Longitude) and the year is 2015. The monthly-mean thermal tropopause pressure is used to separate  
 222 tropospheric and stratospheric O<sub>3</sub> for the model results and satellite observations.

223 A High-resolution Air Quality Reanalysis Dataset over China (CAQRA, Kong, et al., 2020; Tang et al.,  
 224 2020 a, b) is used to evaluate the simulated present-day surface O<sub>3</sub> over China  
 225 (<https://doi.org/10.11922/sciencedb.00053>). This dataset is generated by assimilating surface  
 226 observations from the China National Environmental Monitoring Centre (CNEMC) into the Nested Air  
 227 Quality Prediction Modeling System (Tang et al., 2011, Wang et al., 2000), and it provides self-consistent  
 228 concentration fields of O<sub>3</sub> in China from 2013 to 2019 at high spatial (15 km) and temporal (1 h)  
 229 resolutions. The year used in this study is 2015.

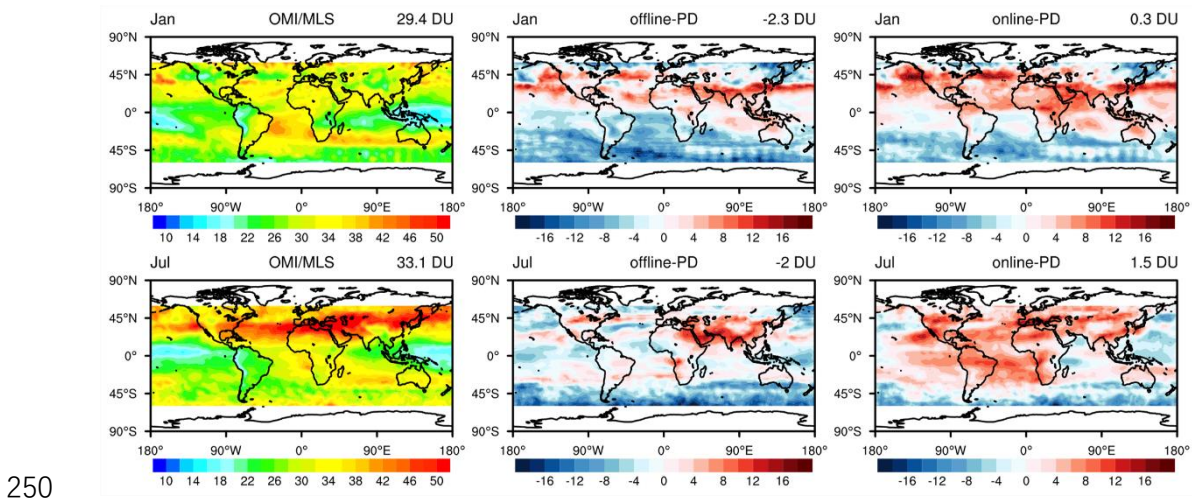
230 In addition, monthly observational surface O<sub>3</sub> concentration are taken from 12 regional stations of the  
 231 Acid Deposition Monitoring Network in East Asia (EANET; <https://www.eanet.asia/>) for 2015: Rishiri,  
 232 Ochiishi, Tappi, Sado-Seki, Happo, Oki, Yusuhara, Hedo, Mondy, Listvyanka, Kanghwa, and Cheju.  
 233 The locations and altitudes of these sites are shown in Figure S2.

234 **3. Tropospheric ozone evaluation**

235 We compared the simulated monthly mean tropospheric column O<sub>3</sub> (TCO) with that derived from  
 236 OMI/MLS for January and July in 2015 (Figure 2). The model captures the general features of the  
 237 observed tropospheric column, reproducing the seasonal pattern, with a minimum of 15 DU at 180°E in

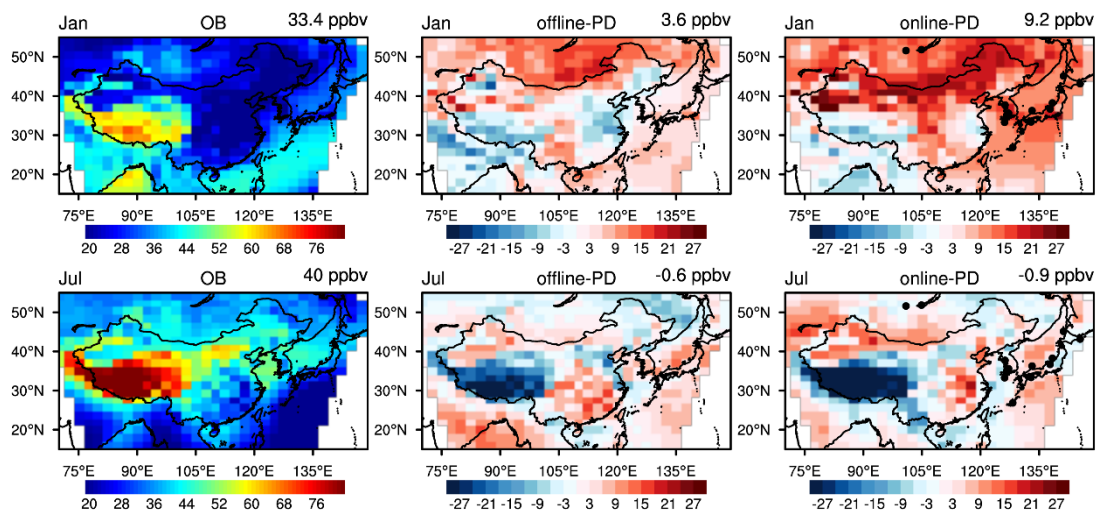


238 the tropics during January and a maximum of >50 DU in northern hemisphere mid-latitudes during July.  
 239 The highest values in the northern mid-latitudes are overestimated in both offline and online simulations,  
 240 especially during July. In the simulations, TCO was calculated by integrating the O<sub>3</sub> from the surface to  
 241 the tropopause. Some of the differences between the simulated TCO and OMI/MLS may be due to the  
 242 relatively coarse vertical resolution of the model (26 levels in online simulations and 56 levels in offline  
 243 simulations). Uncertainty in the satellite dataset (exceeding 5 DU in high latitudes, Ziemke et al. 2011)  
 244 might also contribute to these differences. The accuracy of the emissions inventory also affects the  
 245 simulation results, especially at the surface. The global (60°S~60°N) annual mean tropospheric O<sub>3</sub>  
 246 columns from the offline and online simulations are 29.0 and 32.3 DU, respectively, which match those  
 247 from OMI/MLS (31.7 DU) and the ACCMIP models mean value (30.8 DU, Young et al., 2013) well.  
 248 The online simulated tropospheric ozone column on global annual average is the highest, due to the  
 249 coarser vertical resolution in online simulation (Lamarque et al., 2012).



250

251 Figure 2 Tropospheric column O<sub>3</sub> (DU) from OMI/MLS (left), and the biases of offline (middle) and  
 252 online (right) simulations for January and July under present day conditions. The biases are simulated  
 253 result minus satellite (OML/MLS) result. The values in the right corner of each sub-figure are the  
 254 average over the globe (-60°S to 60°N).



255

256 Figure 3 Surface O<sub>3</sub> mixing ratios in East Asia (ppbv) from the CAQRA reanalysis (left) and the biases  
257 from offline (middle) and online (right) present day simulations in January and July. The biases are  
258 simulations minus observations, and black dots show the locations of EANET observation sites. The  
259 values in the right corner of each sub-figure are the regional mean for East Asia (15~55°N, 70~149°E).

260 As shown in Figure 3, surface O<sub>3</sub> shows substantial seasonal variations with low concentrations in winter  
261 and high concentrations in summer. The spatial distributions of simulated surface O<sub>3</sub> concentrations  
262 match the observations well. The online simulated surface O<sub>3</sub> (ppbv) is overestimated by 9.2 ppbv on  
263 average in winter, especially in Mongolia, north and middle of China, Korea, and Japan, while the offline  
264 simulation is much closer to the observation with a bias of 3.6 ppbv. The coarser resolution of the online  
265 model is likely a reason for its higher bias. The comparison of simulated surface O<sub>3</sub> (ppbv) with EANET  
266 observations show that the simulations reproduce the seasonal variations at these 12 sites (Figure S2 in  
267 the Supplementary Material). In general, the performance of these simulations is very similar to those  
268 from other chemical model studies (Li et al., 2019; Young et al., 2018).

#### 269 **4 Tropospheric ozone budgets and distributions under the Net Zero scenario**

270 An overview of the global model diagnostics for the simulation experiments is given in Table 4. The  
271 tropospheric O<sub>3</sub> burden and budget terms for present-day conditions in this study match previous results  
272 well. Under net zero, the chemical production decreases from 5038 to 3392 Tg(O<sub>3</sub>) yr<sup>-1</sup>, and the chemical  
273 loss decreases from 4641 to 3311 Tg(O<sub>3</sub>) yr<sup>-1</sup>. The net chemical tendency of tropospheric O<sub>3</sub> (NetChem  
274 in Table 4) drops substantially, decreasing from the current 397 Tg(O<sub>3</sub>) yr<sup>-1</sup> to 81 Tg(O<sub>3</sub>) yr<sup>-1</sup>, due to the  
275 large reduction in O<sub>3</sub> precursor emissions (Table 2). This results in an increase in the lifetime of  
276 tropospheric O<sub>3</sub> from 20 days to 22 days. The residual term, which principally reflects net transport from  
277 the stratosphere, increases from the current 595 to 626 Tg(O<sub>3</sub>) yr<sup>-1</sup>. The global tropospheric O<sub>3</sub> burden  
278 decreases by about 20%, from 316 Tg to 247 Tg, bringing it close to the mean burden of 239±22 Tg  
279 estimated for the pre-industrial period (Young et al., 2013, Griffiths et al., 2021). The burden of O<sub>3</sub> of  
280 stratospheric origin in the troposphere (O<sub>3</sub>S) increases from 69 Tg to 77 Tg. This increased stratospheric  
281 contribution may be due to the enhancement of stratospheric circulation and increased stratosphere-  
282 troposphere exchange caused by climate change (Sudo et al., 2003; Lu et al., 2019), and has been seen  
283 in previous studies (e.g., Zanis et al., 2022). In addition, the longer chemical lifetime allows stratospheric  
284 O<sub>3</sub> to persist for longer in the troposphere, enhancing the stratospheric contribution. Compared with pre-  
285 industrial conditions (Griffiths et al., 2021; Table 4), the net chemical production rate is slower, while  
286 the stratospheric contribution is higher. This may indicate that anthropogenic influence is somewhat  
287 weaker than that in the pre-industrial. Compared with other SSP scenarios, particularly the much-studied  
288 SSP3-7.0 pathway (Liu et al., 2022; Griffiths et al., 2021), SSP1-1.9 provides a more positive perspective  
289 on the opportunities for controlling future tropospheric O<sub>3</sub>, and the benefits for air quality.

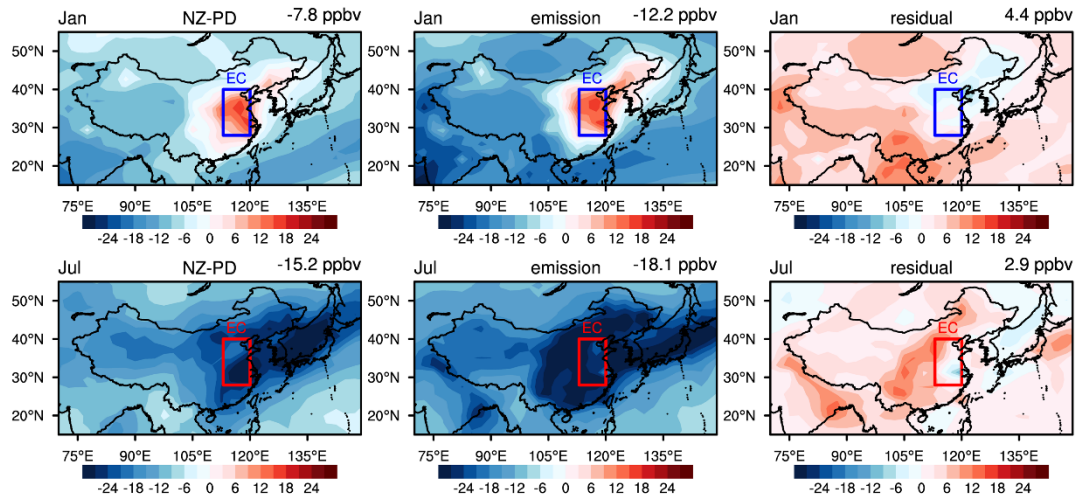
290 Over East Asia, the net photochemical production of tropospheric O<sub>3</sub> also decreases significantly, from  
291 the current 227 Tg(O<sub>3</sub>) yr<sup>-1</sup> to 137 Tg(O<sub>3</sub>) yr<sup>-1</sup> under net zero, but the reduction is less than the global  
292 average and this is attributed to the higher emissions and smaller reductions in precursors over East Asia.  
293 The negative “Residual” budget term for East Asia indicates that the production is larger than the sink,

294 and the total contribution of vertical and horizontal transport from outside of East Asia is negative. This  
 295 indicates that there is net outflow from East Asia with transport of tropospheric O<sub>3</sub> to other regions, and  
 296 this outflow is weakened in the future, from 89 Tg(O<sub>3</sub>) yr<sup>-1</sup> under present day conditions to 38 Tg(O<sub>3</sub>) yr<sup>-1</sup>  
 297 under net zero. The tropospheric O<sub>3</sub> burden in East Asia decreases from 25 Tg to 19 Tg, while the  
 298 burden of O<sub>3</sub> from the stratosphere increases slightly from 5 Tg to 6 Tg. The tropospheric O<sub>3</sub> lifetime in  
 299 East Asia is 15 days, slightly lower than the global average due to the faster photochemical processing  
 300 under relatively high anthropogenic emissions. But the increase of ~2 days matches that of the global  
 301 average.

302 Table 4 Global tropospheric O<sub>3</sub> burden (Tg) and budget terms (Tg yr<sup>-1</sup>) in chemical transport models.

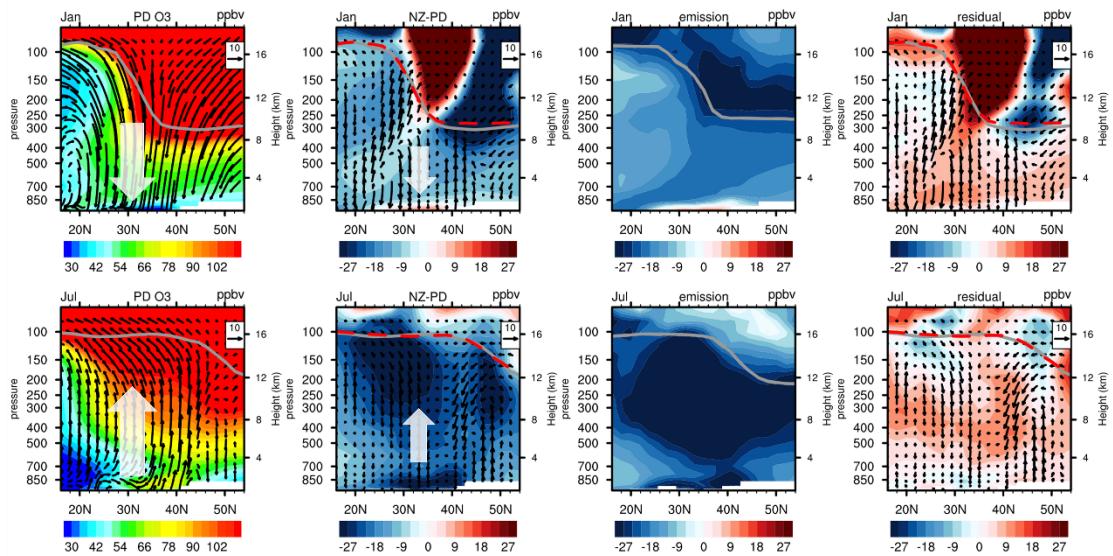
Models	Prod	Loss	NetChem	Residual	DryDep	Burden (O <sub>3</sub> /O <sub>3</sub> S)	Lifetime (days)	Reference
<b>Globe</b>				<b>STE</b>				
33	3948±761	3745±554	245±346	636±273	902±255	307±38	21-25	Wild (2007)
17	4465±514	4114±409	396±247	529±105	949±222	314±33	22±2	Stevenson et al. (2006)
15	5110±606	4668±727	442±309	552±168	1003±200	344±39	22±2	Young et al. (2013)
PI	2549	2437	112	415	528	241	29	Griffiths et
PD	4510	3948	562	284	846	337	26	al. (2021)
<b>PD</b>	<b>5038</b>	<b>4641</b>	<b>397</b>	<b>595</b>	<b>992</b>	<b>316/69</b>	<b>20</b>	<b>This study</b>
<b>NZ</b>	<b>3392</b>	<b>3311</b>	<b>81</b>	<b>626</b>	<b>707</b>	<b>247/77</b>	<b>22</b>	<b>This study</b>
<b>East Asia</b>				<b>Transport</b>				
<b>PD</b>	<b>682</b>	<b>455</b>	<b>227</b>	<b>-89</b>	<b>138</b>	<b>25/5</b>	<b>15</b>	<b>This study</b>
<b>NZ</b>	<b>430</b>	<b>293</b>	<b>137</b>	<b>-38</b>	<b>99</b>	<b>19/6</b>	<b>17</b>	<b>This study</b>

303 Prod for chemical production, Loss for chemical loss, Prod-Loss for net chemical production (NetChem)  
 304 and DryDep for dry deposition; Residual is the term balance by Residual=Loss-Prod+DryDep. Units of  
 305 Prod, Loss, NetChem, Residual and DryDep are in Tg(O<sub>3</sub>) yr<sup>-1</sup>, Burden in Tg(O<sub>3</sub>), and Lifetime in days.  
 306 The climatological pressure tropopause is used. PD is the online present day experiment simulation. NZ  
 307 is the online net zero experiment simulation. The results of Griffiths et al. (2021) are the average of four  
 308 models (UKESM1, CESM2-WACCM, GFDL-ESM4, MRI-ESM2-0), and PD is the average from 1995  
 309 to 2004, while PI (pre-industrial) is the average from 1850 to 1859.



310

311 Figure 4 Changes in surface  $O_3$  mixing ratio (ppbv) over China in January and July between present  
 312 day and net zero (online-NZ minus online-PD, left), and changes due to emissions (offline-NZ minus  
 313 offline-PD, middle) and the residual (left minus middle panel, right). The values in the right corner of  
 314 each panel are the regions mean over East Asia ( $15^\circ\sim 55^\circ N$ ,  $70^\circ\sim 149^\circ E$ ). The frame is the region of  
 315 Eastern China (EC,  $28^\circ\sim 40^\circ N$ ,  $113^\circ\sim 120^\circ E$ ).



316

317 Figure 5 Zonal mean  $O_3$  cross section (ppbv) and wind speed (vectors,  $v: m s^{-1}$ ,  $w: (-500) pa s^{-1}$ ) over  
 318 Eastern China (longitudes  $111\sim 122^\circ E$ ) in January and July under present day (online-PD, left), the  
 319 changes in  $O_3$  and wind speed (second panels) and changes due to emissions (third panels) and the  
 320 residual (second panels minus third panels, right). Grey lines show the tropopause location under  
 321 present day conditions; the red dashed lines show the tropopause location under net zero.

322 The changes in surface  $O_3$  over East Asia between 2015 and 2060 in winter and summer are shown in  
 323 Figure 4. The left panels show the changes in surface  $O_3$  under net zero (online-NZ minus online-PD),  
 324 which include the effects of climate change and emissions changes. The climate change in this study

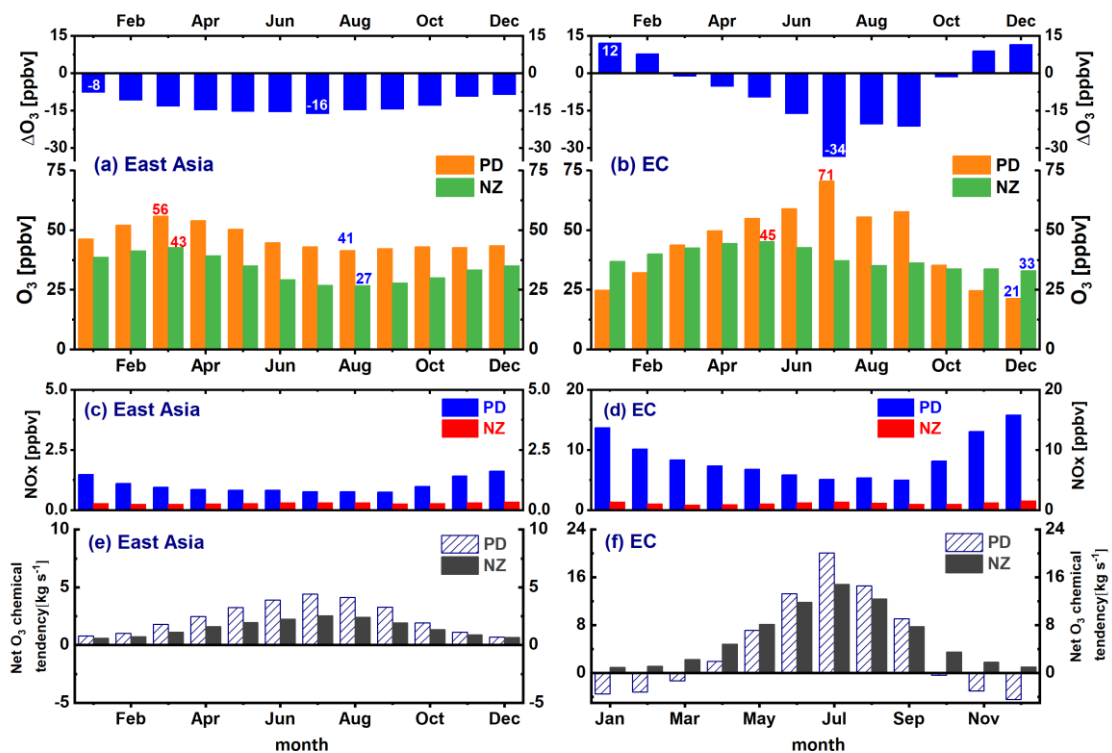
325 includes changes in atmospheric parameters (air temperature, relative humidity, atmospheric circulation  
326 etc.) from the free-run of atmospheric simulation experiments (online). The climate change along SSP119  
327 is much weaker than other pathways, and the change in global surface air temperature in this study is not  
328 significant (Figure S3 in Supplementary Material). Over East Asia, the surface air temperature is  
329 increased by an annual average of 0.2°C. The middle panels show the changes in surface O<sub>3</sub> under the  
330 effect of emissions changes only (offline-NZ minus offline-PD). The right panels show the residual  
331 changes in surface O<sub>3</sub> which reflect the effect of climate change, but are also influenced by differences  
332 in model setup between the online and offline simulations (left panels minus middle panels). Surface O<sub>3</sub>  
333 decreases in East Asia under net zero, with a mean reduction of 7.7 ppbv in winter and a greater reduction  
334 of 16.2 ppbv in summer. Turnock et al. (2019) estimated an annual mean reduction of 8 ppbv in 2050  
335 along the SSP1-1.9 pathway, slightly less than we find here. However, we have used the more stringent  
336 DPEC Ambitious-pollution-Neutral-goals emission scenario for China rather than the standard SSP1-1.9  
337 pathway and we note that anthropogenic NO emissions in China are 1.5 Tg (NO) yr<sup>-1</sup> lower in this  
338 scenario than those in SSP1-1.9. Surface O<sub>3</sub> over Eastern China and South Korea increases in winter in  
339 these scenarios, driven by the reduction in emissions (left and middle panels). This increase in surface  
340 O<sub>3</sub> is caused by a weakening of titration under lower regional NO emissions in the future. The influence  
341 of climate change on surface O<sub>3</sub> is relatively weak and leads to an increase of surface O<sub>3</sub> in most parts of  
342 East Asia (right panels). This is partly due to enhanced vertical circulation leading to an increased  
343 contribution from stratospheric O<sub>3</sub> (Akritidis et al., 2019; shown in Figure S4) and the photochemical  
344 change under warmer climate (Zanis et al., 2022). Xu et al. (2022) also showed that emission reduction  
345 is far more effective than climate change in improving air quality (PM<sub>2.5</sub> and O<sub>3</sub>) over East Asia under a  
346 carbon neutral reduction pathway. Here we will use tagging simulations to quantify the contributions of  
347 different sources to surface O<sub>3</sub> changes over East Asia, especially over Eastern China where surface O<sub>3</sub>  
348 increases in winter and decreases in summer.

349 It can be seen from the vertical distribution of O<sub>3</sub> and circulation (shown in the first panels of Figure 5)  
350 that the O<sub>3</sub> concentration increases with altitude under present day conditions. At the same altitude, the  
351 O<sub>3</sub> concentration is higher in middle and high latitudes than in low latitudes. In winter, there is strong net  
352 descent of air over eastern China (30~40°N), which weakens in spring, and turns to updraft in summer.  
353 These may be due to the weakened Brewer-Dobson circulation and strengthened convection (Butchart,  
354 2014; Wild and Akimoto, 2001). As shown in the second panels of Figure 5, there is a net decrease in  
355 tropospheric O<sub>3</sub> in future, with an increase only seen near 30°N very close to the surface. In summer, the  
356 reduction in tropospheric O<sub>3</sub> is greatest, especially near the tropopause where it exceeds 30 ppbv. In  
357 addition, due to the temperature increase and circulation enhancement in the future, the tropopause height  
358 increases, especially in the mid-latitude region in winter where the increase is about 7 hPa. As seen from  
359 the third panels of Figure 5, the reduction of emissions from aircraft (NO emissions in Figure S1) leads  
360 to a reduction in O<sub>3</sub> production, and the O<sub>3</sub> concentration near the tropopause decreases substantially in  
361 the future. However, other factors such as climate change (the fourth panel in Figure 5) lead to increases  
362 in tropospheric O<sub>3</sub> by 2060.

363 **5 The contribution of O<sub>3</sub> chemistry and intercontinental transport**

364 Surface O<sub>3</sub> shows substantial seasonal variation over East Asia with a peak in spring, as shown in Figure  
 365 6a. It reaches a maximum (56 ppbv) in March and is lowest (41 ppbv) in August under present day  
 366 conditions. Under net zero, the concentration of surface O<sub>3</sub> is lower throughout the year, and while the  
 367 peak is still in March, the mixing ratio drops to 43 ppbv. The decrease is greatest in July, 16 ppbv, which  
 368 reflects weaker chemical production in summertime under lower future emissions (Figure 6e). In contrast,  
 369 surface O<sub>3</sub> over Eastern China is highest (71 ppbv) in July and lowest (21 ppbv) in December under  
 370 present day conditions (Figure 6b). Under net zero, surface O<sub>3</sub> increases in winter and decreases in  
 371 summer, and the peak shifts from July to May, due to the changes in O<sub>3</sub> precursors emissions (Bowman  
 372 et al., 2021). This shifts the seasonal peak from summer towards spring, when it is more greatly  
 373 influenced by stratosphere-troposphere exchange. The decrease is highest in July, as seen over the wider  
 374 East Asian region, but is twice as large, at 34 ppbv, reflecting the stronger present-day emissions over  
 375 Eastern China. There is a substantial increase in O<sub>3</sub> in January of 12 ppbv, reflecting reduced titration by  
 376 NO. The concentration of surface NO<sub>x</sub> decreases more than 60%, and by an even larger factor in winter  
 377 (~90%, 14 ppbv); and its seasonal variation is reduced which accounts for the reduction in anthropogenic  
 378 emissions (Figure 6d). In terms of the O<sub>3</sub> chemical budget, local chemical production and destruction are  
 379 both reduced in the future. The peak in net O<sub>3</sub> chemical production still occurs in summer which  
 380 highlights that photochemical processes continue to dominate the seasonal variation of surface O<sub>3</sub> in  
 381 Eastern China in future (Figure 6f). However, the net chemical destruction that currently occurs in winter  
 382 is replaced with a small net O<sub>3</sub> production, reflecting the reduced titration of O<sub>3</sub> by NO under future  
 383 emissions, which are very greatly reduced under net zero (Liu et al., 2022, 2023).

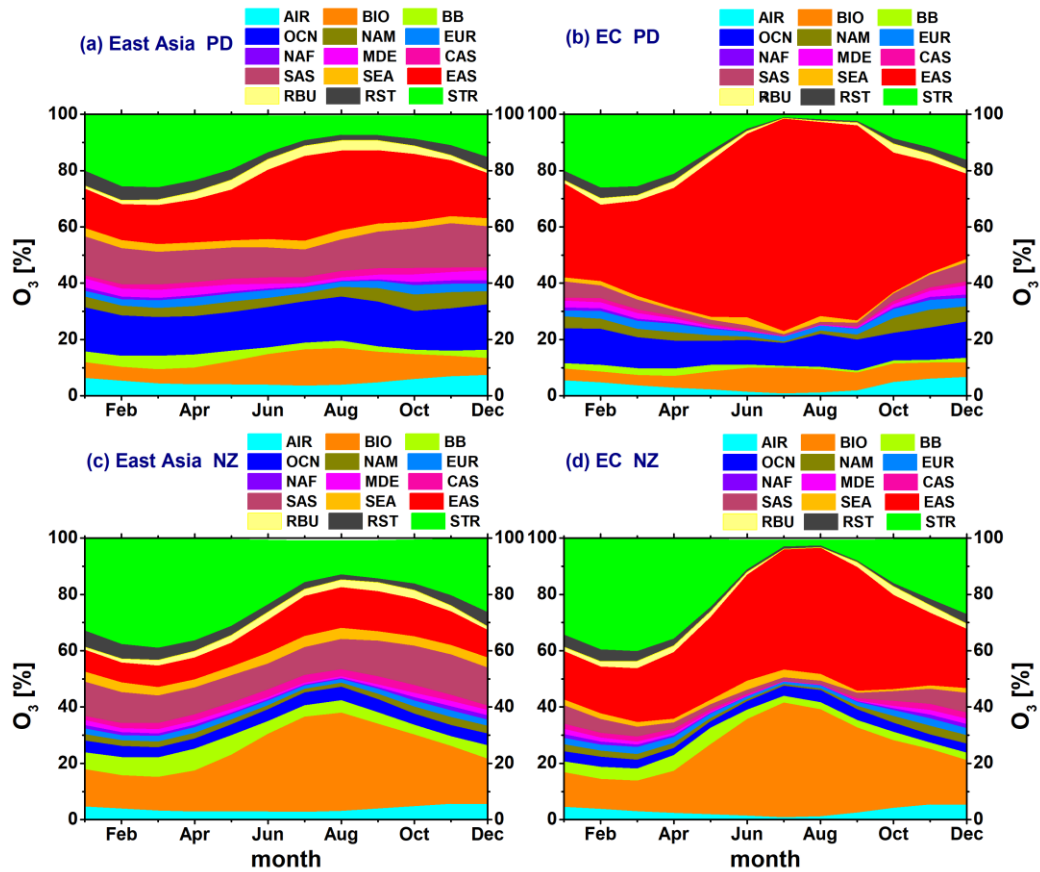
384



385

386 Figure 6 Comparison of O<sub>3</sub> (a, b), NO<sub>x</sub> (c, d) and net O<sub>3</sub> chemical tendency (e, f) at the surface under  
387 present day and net zero conditions over East Asia (left) and Eastern China (right). Results are from the  
388 online simulations (online-PD and online-NZ). Maximum and minimum O<sub>3</sub> mixing ratios are  
389 highlighted in red and blue, respectively, and the largest and smallest O<sub>3</sub> changes are indicated in  
390 white. The net O<sub>3</sub> chemical tendency is the net photochemical production rate of O<sub>3</sub> (kg s<sup>-1</sup>).

391 We quantify the contributions of regional transport and stratospheric input to surface O<sub>3</sub> on a monthly  
392 basis in Figure 7. In present day (Figure 7a), we find that the contribution of anthropogenic NO emissions  
393 from East Asia (EAS) is highest, especially in summer when it reaches 30% (12 ppbv in Figure 8). The  
394 total contributions from anthropogenic NO emissions outside East Asia (EAS\_out, without ocean) is 33%  
395 (16 ppbv) on average with little seasonal variation, and it is highest over South Asia (SAS), accounting  
396 for 12% (6 ppbv). The contribution from biogenic NO emissions from soils (BIO) is also important,  
397 exceeding 10% (5 ppbv in Figure 8) in summer. The contributions from the ocean (OCN) show little  
398 seasonal variation, contributing 15% (6 ppbv). Under net zero (Figure 7c), the anthropogenic contribution  
399 from East Asia drops dramatically, to 14% (4 ppbv in Figure 8) in summer, due to the reduced emissions  
400 of O<sub>3</sub> precursors. The total contributions from anthropogenic NO emissions outside East Asia decrease  
401 to 28% (10 ppbv) on average, 7 ppbv in summer (in Figure 8). The contribution of biogenic sources is  
402 enhanced, and forms the dominant contributor to surface O<sub>3</sub> under net zero, especially in summer, ~40%  
403 (9 ppbv in Figure 8). The emissions from biogenic sources do not vary from year to year in this study.  
404 The enhanced contribution of biogenic sources is mainly due to the increased O<sub>3</sub> production efficiency,  
405 which is a consequence of lower O<sub>3</sub> precursor concentrations (Kleinman et al., 2002; Zaveri et al., 2003).  
406 The contribution of oceanic sources decreases to 4% (1 ppbv) due to reduced emissions from shipping.  
407 The contribution from stratospheric O<sub>3</sub> (STR) is highest in March (26%, 14 ppbv), and lowest in August  
408 (7%, 3 ppbv) under present day conditions. Under net zero, the highest contribution is increased to 39%  
409 (17 ppbv), and the lowest contribution is also increased, to 12% (3 ppbv). This may be due to enhanced  
410 stratospheric circulation, slower photochemical loss and a longer lifetime of O<sub>3</sub> in the troposphere  
411 allowing greater transport of stratospheric O<sub>3</sub> to the ground.



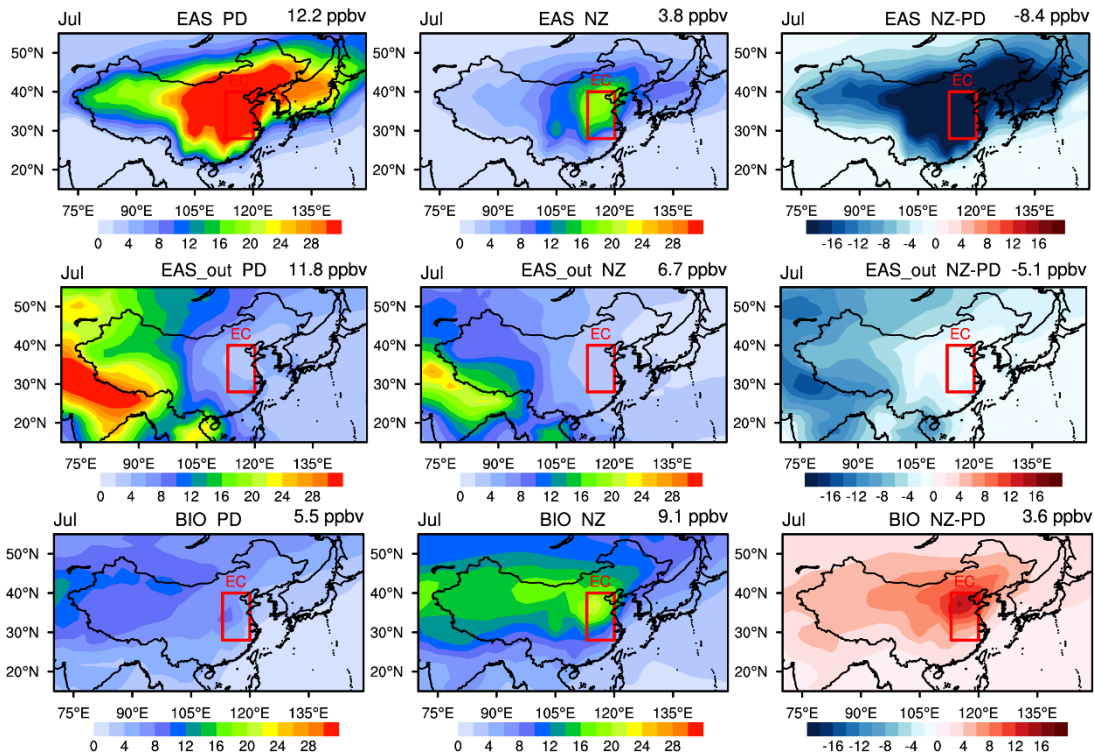
412

413 Figure 7 Contributions of different sources to surface O<sub>3</sub> under present day and net zero conditions over  
 414 East Asia (a, c) and Eastern China (b, d). Results are from the online simulations (online-PD and  
 415 online-NZ). 11 geographical source regions are used for anthropogenic NO<sub>x</sub> emission. BIO, BB, AIR,  
 416 and LIG are the contribution of NO<sub>x</sub> emission from biogenic sources, biomass burning, aircraft and  
 417 lightning to O<sub>3</sub>. STR is the contribution of O<sub>3</sub> originating in the stratosphere.

418 Over Eastern China (Figure 7b), the contribution from East Asian anthropogenic sources is highest,  
 419 especially in summer when it exceeds 70% (43 ppbv, shown in Figure 8). The total contributions from  
 420 anthropogenic NO emissions out of East Asia is 16% (6 ppbv) on average, 4 ppbv in summer (in Figure  
 421 8). Biogenic and oceanic sources make a smaller contribution over this region, only 6% (3 ppbv) and 10%  
 422 (5 ppbv) on average, respectively. Under net zero (Figure 7d), the contribution of East Asian  
 423 anthropogenic sources drops to 42% (16 ppbv) in summer, but remains the dominant source of surface  
 424 O<sub>3</sub> in Eastern China. The total contributions from anthropogenic NO emissions outside East Asia show  
 425 little change. The contribution of biogenic sources is enhanced, especially in summer, reaching 40% (14  
 426 ppbv in Figure 8), close to the contribution from East Asian sources. The stratospheric contribution is  
 427 highest in early spring (25%, 11 ppbv), and lowest in summer (2%, 1 ppbv). Under net zero, the  
 428 stratospheric contribution is enhanced to 40% (17 ppbv) in March and 3% (1 ppbv) in summer, similar  
 429 to the seasonal contributions over East Asia. In addition, the high NO concentration in heavily urbanized  
 430 Eastern China has a titration effect on O<sub>3</sub>, but the strong future decreases in NO weaken this effect,  
 431 reducing the loss of stratospheric O<sub>3</sub> as well as O<sub>3</sub> from local sources. Overall, surface O<sub>3</sub> shows



432 substantial decreases through much of the year, and the local contribution is reduced, which highlights  
 433 the beneficial role that net zero policies may have for controlling surface O<sub>3</sub> pollution in China.



434  
 435 Figure 8 The contributions of anthropogenic NO emissions over East Asia (EAS, first row), outside  
 436 East Asia (EAS\_out, second row), and biogenic emission (BIO, third row) on surface O<sub>3</sub> (ppbv) over  
 437 East Asia in July of present day (online-PD, left) and net zero (online-NZ, middle), and the differences  
 438 between PD and NZ (online-NZ minus online-PD, right). The values in the right corner of each sub-  
 439 figure are the regional mean over East Asia. The box shows the region of Eastern China.

440 **6 Summary and conclusions**

441 We quantify tropospheric O<sub>3</sub> budgets, spatiotemporal distributions of future surface O<sub>3</sub> in East Asia and  
 442 regional O<sub>3</sub> source contributions for 2060 under a net zero scenario, using the NCAR Community Earth  
 443 System Model (CESM) and online O<sub>3</sub> tagging methods. The simulated monthly mean global tropospheric  
 444 column O<sub>3</sub> and surface O<sub>3</sub> mixing ratios over East Asia capture the general features in observations well  
 445 under present day conditions. The offline simulations perform better than online simulations, as the  
 446 nudging provides a closer match to observed meteorological conditions. The tropospheric O<sub>3</sub> burden and  
 447 budget terms under present-day conditions in this study also matches those of previous model studies  
 448 well.

449 The simulated tropospheric O<sub>3</sub> burden is likely to decrease from 316 Tg under present day conditions to  
 450 247 Tg by 2060 under the net zero scenario. This brings it close to that found in previous studies under  
 451 preindustrial conditions of  $239 \pm 22$  Tg (Young et al., 2013). Future tropospheric O<sub>3</sub> chemical production  
 452 and loss are both reduced, and the net chemical tendency decreases from 397 to 81 Tg(O<sub>3</sub>) yr<sup>-1</sup>. The  
 453 contribution of stratospheric O<sub>3</sub> increases from 69 to 77 Tg, due to enhancement of atmospheric

454 circulation and increased stratosphere-troposphere exchange caused by climate change and the longer  
455 chemical lifetime of stratospheric O<sub>3</sub> in the troposphere under decreased anthropogenic emissions of  
456 pollutants. The mean tropospheric lifetime of O<sub>3</sub> is increased by 2 days, ~10%. Over East Asia, one of  
457 the highest anthropogenic emissions regions, the O<sub>3</sub> burden decreases from 25 to 19 Tg, and the net  
458 chemical tendency drops from 227 to 137 Tg(O<sub>3</sub>) yr<sup>-1</sup>. East Asia is a region of net O<sub>3</sub> production, and the  
459 outflow is expected to decrease from 89 to 38 Tg(O<sub>3</sub>) yr<sup>-1</sup>. The burden of O<sub>3</sub> from the stratosphere  
460 increases from 5 to 6 Tg. The lifetime of tropospheric O<sub>3</sub> over East Asia is shorter than the global average,  
461 ~15 days, due to the high anthropogenic emissions, but increases by 2 days, similar to the global mean.  
462 Compared with other SSP scenarios, particularly the much-studied SSP3-7.0 pathway, SSP1-1.9 provides  
463 a more positive perspective on the opportunities for controlling future tropospheric O<sub>3</sub>, and the benefits  
464 for the improvement of air quality.

465 Regional average surface O<sub>3</sub> decreases throughout the year over East Asia, with highest decreases in  
466 summer (16 ppbv) in the future under the net zero scenario. Over Eastern China, the peak in surface O<sub>3</sub>  
467 shifts from July to May. Surface O<sub>3</sub> decreases strongly in July (34 ppbv), and increases in winter,  
468 especially in January, 12 ppbv. The increased O<sub>3</sub> in winter is caused by reduced titration of O<sub>3</sub> by NO  
469 associated with lower anthropogenic NO emissions and by enhanced stratospheric input. The  
470 tropospheric O<sub>3</sub> over most regions decreases due to the large decrease in O<sub>3</sub> precursors emissions.  
471 Climate change leads to only a small increase in tropospheric O<sub>3</sub> under this scenario. Local anthropogenic  
472 emissions play a dominant role in controlling O<sub>3</sub> changes over East Asia in summer, but this will drop  
473 substantially from 30% in present day to 14% under net zero. The contribution of biogenic sources is  
474 enhanced, and forms the dominant contributor to future surface O<sub>3</sub>, especially in summer, ~40%. This  
475 enhanced contribution of biogenic sources is due here to increased O<sub>3</sub> production efficiency associated  
476 with reduced O<sub>3</sub> precursors concentrations, but may be underestimated if biogenic emissions also  
477 increase in future as expected. The lower extent of climate change along SSP119 leads to relatively little  
478 impact on tropospheric O<sub>3</sub> under net zero, while the emission reductions associated with net zero policies  
479 are sufficient to mitigate surface O<sub>3</sub> pollution over East Asia, especially in summer.

480 The combined emissions and O<sub>3</sub> tagging method used here provides a reliable way to quantify the  
481 changes of tropospheric O<sub>3</sub> and its sources in future under a net zero scenario. The results of this study  
482 clarify the separate impacts of climate change and emissions on tropospheric O<sub>3</sub> changes over East Asia,  
483 and highlight the significance of controlling O<sub>3</sub> precursors emissions along the net zero scenario,  
484 especially anthropogenic emissions. The reduction of anthropogenic O<sub>3</sub> precursor emissions should be  
485 the most effective way to control the increase of tropospheric O<sub>3</sub>, and this requires joint efforts on a  
486 global scale.

487

## 488 **Acknowledgements**

489 Xuewei Hou acknowledges the High-Performance Computing Center, Nanjing University of Information  
490 Science and Technology for the high-performance computing system. The authors would like to thank

491 Prof. Tim Butler and Dr. Aurelia Lupascu at the Institute for Advanced Sustainability Studies (now the  
492 Research Institute for Sustainability) in Potsdam, Germany for helping us to update the TOAST source  
493 attribution code in the CESM model. Thank Dr. Yongjie Huang (IAP/CAS) for providing map database  
494 (<https://github.com/huangynj/NCL-Chinamap.git>).

#### 495 **Financial support**

496 This study was supported by the National Key Research and Development Program of China (Grant No.,  
497 2022YFC3701204), the National Natural Science Foundation of China (Grant No., 42021004 and  
498 42275115), and Key Laboratory of Atmospheric Chemistry, China Meteorological Administration  
499 (LAC/CMA, Grant No., 2023B05). OW and JL acknowledge support from the UK-China collaboration  
500 to optimize net-zero policy options for air quality and health (COP-AQ) under grant 2021GRIP02COP-  
501 AQ.

#### 502 **Data availability**

503 CAQRA can be freely downloaded at <https://doi.org/10.11922/sciencedb.00053>, and the prototype  
504 product, which contains the monthly and annual means of the CAQRA dataset, is available at  
505 <https://doi.org/10.11922/sciencedb.00092>. The simulated O<sub>3</sub> data generated in this study are available on  
506 <https://doi.org/10.5281/zenodo.8137796>.

#### 507 **Author contribution**

508 XH, OW, and BZ jointly developed the concept for this study. XH set up the model, conducted the  
509 simulations and data analysis. XH and OW contributed to the writing. BZ and JL discussed the results  
510 and offered valuable comments.

#### 511 **Competing interests**

512 The authors declare that they have no conflict of interest.

#### 513 **Review statement**

514 This paper was edited by Bryan N. Duncan and reviewed by two anonymous referees.

515

#### 516 **References:**

517 Akritidis, D., Pozzer, A., and Zanis, P.: On the impact of future climate change on tropopause folds and  
518 tropospheric ozone, *Atmos. Chem. Phys.*, 19, 14387–14401, [https://doi.org/10.5194/acp-19-14387-](https://doi.org/10.5194/acp-19-14387-2019)  
519 2019, 2019.

520 Allen, R. J., Turnock, S., Nabat, P., Neubauer, D., Lohmann, U., Olivié, D., Oshima, N., Michou, M.,  
521 Wu, T., Zhang, J., Takemura, T., Schulz, M., Tsigaridis, K., Bauer, S. E., Emmons, L., Horowitz, L.,  
522 Naik, V., van Noije, T., Bergman, T., Lamarque, J.-F., Zanis, P., Tegen, I., Westervelt, D. M., Le

- 523 Sager, P., Good, P., Shim, S., O'Connor, F., Akritidis, D., Georgoulas, A. K., Deushi, M., Sentman,  
524 L. T., John, J. G., Fujimori, S., and Collins, W. J.: Climate and air quality impacts due to mitigation  
525 of non-methane near-term climate forcers, *Atmos. Chem. Phys.*, 20, 9641–9663,  
526 <https://doi.org/10.5194/acp-20-9641-2020>, 2020.
- 527 Bowman, H., Turnock, S., Bauer, S. E., Tsigaridis, K., Deushi, M., Oshima, N., O'Connor, F. M.,  
528 Horowitz, L., Wu, T., Zhang, J., Kubistin, D., and Parrish, D. D.: Changes in anthropogenic precursor  
529 emissions drive shifts in the ozone seasonal cycle throughout the northern midlatitude troposphere,  
530 *Atmos. Chem. Phys.*, 22, 3507–3524, <https://doi.org/10.5194/acp-22-3507-2022>, 2022.
- 531 Butchart, N.: The Brewer-Dobson circulation, *Reviews of Geophysics*, 52(2), 157-184,  
532 <https://doi.org/10.1002/2013RG000448>, 2014.
- 533 Butchart, N., Charlton-Perez, A. J., Cionni, I., Hardiman, S. C., Haynes, P. H., Kruger, K., Kushner, P.  
534 J., Newman, P. A., Osprey, S. M., Perlwitz, J., Sigmond, M., Wang, L., Akiyoshi, H., Austin, J.,  
535 Bekki, S., Baumgaertner, A., Braesicke, P., Bruhl, C., Chipperfield, M., Dameris, M., Dhomse, S.,  
536 Eyring, V., Garcia, R., Garny, H., Jockel, P., Lamarque, J.-F., Marchand, M., Michou, M.,  
537 Morgenstern, O., Nakamura, T., Pawson, S., Plummer, D., Pyle, J., Rozanov, E., Scinocca, J.,  
538 Shepherd, T. G., Shibata, K., Smale, D., Teyssedre, H., Tian, W., Waugh, D. and Yamashita, Y.:  
539 Multi-model climate and variability of the stratosphere, *J. Geophys. Res.*, 116, D05102,  
540 <https://doi.org/10.1029/2010JD014995>, 2011.
- 541 Butler, T., Lupascu, A., Coates, J., and Zhu, S.: TOAST 1.0: Tropospheric Ozone Attribution of Sources  
542 with Tagging for CESM 1.2.2, *Geosci. Model Dev.*, 11, 2825–2840, [https://doi.org/10.5194/gmd-11-](https://doi.org/10.5194/gmd-11-2825-2018)  
543 [2825-2018](https://doi.org/10.5194/gmd-11-2825-2018), 2018.
- 544 Butler, T., Lupascu, A. and Nalam A.: Attribution of ground-level ozone to anthropogenic and natural  
545 sources of nitrogen oxides and reactive carbon in a global chemical transport model, *Atmos. Chem.*  
546 *Phys.*, 20, 10707–10731, <https://doi.org/10.5194/acp-20-10707-2020>, 2020.
- 547 Cheng, J., Tong, D., Zhang, Q., Liu, Y., Lei, Y., Yan, G., Yan, L., Yu, S., Cui, R. Y., Clarke, L., Geng,  
548 G. N., Zheng, B., Zhang, X. Y., Davis, J. S., and He, K. B.: Pathways of China's PM<sub>2.5</sub> air quality  
549 2015–2060 in the context of carbon neutrality, *Natl. Sci. Rev.*, nwab078,  
550 <https://doi.org/10.1093/nsr/nwab078>, 2021.
- 551 Cionni, I., Eyring, V., Lamarque, J.F., Randel, W.J., Stevenson, D.S., Wu, F., Bodeker, G.E., Shepherd,  
552 T.G., Shindell, D.T., Waugh, D.W.: Ozone database in support of CMIP5 simulations: results and  
553 corresponding radiative forcing, *Atmos. Chem. Phys.*, 11, 11267–11292. [https://doi.org/10.5194/acp-](https://doi.org/10.5194/acp-11-11267-2011)  
554 [11-11267-2011](https://doi.org/10.5194/acp-11-11267-2011), 2011.
- 555 Danabasoglu, G., Lamarque, J. -F., Bacmeister, J., Bailey, D. A., DuVivier, A. K., Edwards, J., Emmons,  
556 L. K., Fasullo, J., Garcia, R., Gettelman, A., Hannay, C., Holland, M. M., Large, W. G., Lauritzen, P.  
557 H., Lawrence, D. M., Lenaerts, J. T. M., Lindsay, K., Lipscomb, W. H., Mills, M. J., Neale, R., Oleson,  
558 K. W., Otto-Bliesner, B., Phillips, A. S., Sacks, W., Tilmes, S., Kampenhout, L. van, Vertenstein, M.,

559 Bertini, A., Dennis, J., Deser, C., Fischer, C., Fox-Kemper, B., Kay, J. E., Kinnison, D., Kushner, P.  
560 J., Larson, V. E., Long, M. C., Mickelson, S., Moore, J. K., Nienhouse, E., Polvani, L., Rasch, P. J.,  
561 Strand, W. G.: The Community Earth System Model Version 2 (CESM2), *J. Adv. Model. Earth Syst.*,  
562 12(2). <https://doi.org/10.1029/2019MS001916>, 2020.

563 Emberson, L.: Effects of ozone on agriculture, forests and grasslands, *Philosophical Transactions of The*  
564 *Royal Society A Mathematical Physical and Engineering Sciences*, 378(2183), 20190327,  
565 <https://doi.org/10.1098/rsta.2019.0327>, 2020.

566 Emmons, L. K., Walters, S., Hess, P. G., Lamarque, J.-F., Pfister, G. G., Fillmore, D., Granier, C.,  
567 Guenther, A., Kinnison, D., Laepple, T., Orlando, J., Tie, X., Tyndall, G., Wiedinmyer, C., Baughcum,  
568 S. L., and Kloster, S.: Description and evaluation of the Model for Ozone and Related chemical  
569 Tracers, version 4 (MOZART-4), *Geosci. Model Dev.*, 3, 43–67, [https://doi.org/10.5194/gmd-3-43-](https://doi.org/10.5194/gmd-3-43-2010)  
570 2010, 2010.

571 Eyring, V., Bony, S., Meehl, G. A., Senior, C. A., Stevens, B., Stouffer, R. J., and Taylor, K. E.: Overview  
572 of the Coupled Model Intercomparison Project Phase 6 (CMIP6) experimental design and  
573 organization, *Geosci. Model Dev.*, 9, 1937–1958, <https://doi.org/10.5194/gmd-9-1937-2016>, 2016.

574 Fan, X., Duan, Q., Shen, C., Wu, Y., and Xing, C.: Global surface air temperatures in CMIP6: historical  
575 performance and future changes, *Environ. Res. Lett.*, 15, 104056, [https://doi.org/10.1088/1748-](https://doi.org/10.1088/1748-9326/abb051)  
576 9326/abb051, 2020.

577 Griffiths, P. T., Murray, L. T., Zeng, G., Shin, Y. M., Abraham, N. L., Archibald, A. T., Deushi, M.,  
578 Emmons, L. K., Galbally, I. E., Hassler, B., Horowitz, L. W., Keeble, J., Liu, J., Moeni, O., Naik,  
579 V., O'Connor, F. M., Oshima, N., Tarasick, D., Tilmes, S., Turnock, S. T., Wild, O., Young, P. J.,  
580 and Zanis, P.: Tropospheric ozone in CMIP6 simulations, *Atmos. Chem. Phys.*, 21, 4187–4218,  
581 <https://doi.org/10.5194/acp-21-4187-2021>, 2021.

582 Guenther, A. B., Jiang, X., Heald, C. L., Sakulyanontvittaya, T., Duhl, T., Emmons, L. K., and Wang,  
583 X.: The Model of Emissions of Gases and Aerosols from Nature version 2.1 (MEGAN2.1): An  
584 extended and updated framework for modeling biogenic emissions, *Geosci. Model Dev.*, 5(6), 1471–  
585 1492, <https://doi.org/10.5194/gmd-5-1471-2012>, 2012.

586 Guenther, A., Karl, T., Harley, P., Wiedinmyer, C., Palmer, P. I., and Geron, C.: Estimates of global  
587 terrestrial isoprene emissions using MEGAN (Model of Emissions of Gases and Aerosols from  
588 Nature), *Atmos. Chem. Phys.*, 6, 3181–3210, <https://doi.org/10.5194/acp-6-3181-2006>, 2006.

589 Heald, C. L., Henze, D. K., Horowitz, L. W., Feddema, J., Lamarque, J.-F., Guenther, A., Hess, P. G.,  
590 Vitt, F., Seinfeld, J. H., Goldstein, A. H., and Fung, I.: Predicted change in global secondary organic  
591 aerosol concentrations in response to future climate, emissions, and land use change, *J. Geophys.*  
592 *Res.-Atmos.*, 113, D05211, <https://doi.org/10.1029/2007JD009092>, 2008.

593 Hong, C. P., Zhang, Q., Zhang, Y., Davis, S. J., Tong, D., Zheng, Y. X., Liu, Z., Guan, D., He, K. B.,  
594 Schellnhuber, H. J.: Impacts of climate change on future air quality and human health in China, *Proc*  
595 *Natl Acad Sci*, 116(35), 17193–17200, <https://doi.org/10.1073/pnas.1812881116>, 2019.

596 Janssens-Maenhout, G., Crippa, M., Guizzardi, D., Dentener, F., Muntean, M., Pouliot, G., Keating, T.,  
597 Zhang, Q., Kurokawa, J., Wankmüller, R., Denier van der Gon, H., Kuenen, J. J. P., Klimont, Z.,  
598 Frost, G., Darras, S., Koffi, B., and Li, M.: HTAP\_v2.2: a mosaic of regional and global emission  
599 grid maps for 2008 and 2010 to study hemispheric transport of air pollution, *Atmos. Chem. Phys.*, 15,  
600 11411–11432, <https://doi.org/10.5194/acp-15-11411-2015>, 2015.

601 Jerrett, M., Burnett, R.T., Pope, C.A., Ito, K., Thurston, G., Krewski, D., Shi, Y., Calle, E., Thun, M.:  
602 Long-term ozone exposure and mortality, *N. Engl. J. Med.*, 360, 1085–1095.  
603 <https://doi.org/10.1056/NEJMoa0803894>, 2009.

604 Kawase, H., Nagashima, T., Sudo, K., Nozawa, T.: Future changes in tropospheric ozone under  
605 representative concentration pathways (RCPs), *Geophys. Res. Lett.* 38, L05801.  
606 <https://doi.org/10.1029/2010GL046402>, 2011.

607 Karset, I. H. H., Berntsen, T. K., Storelvmo, T., Alterskjær, K., Grini, A., Olivíe, D., Kirkevåg, A., Seland,  
608 Ø., Iversen, T., and Schulz, M.: Strong impacts on aerosol indirect effects from historical oxidant  
609 changes, *Atmos. Chem. Phys.*, 18, 7669–7690, <https://doi.org/10.5194/acp-18-7669-2018>, 2018.

610 Kim, M.J., Park, R.J., Ho, C.-H., Woo, J.-H., Choi, K.-C., Song, C.-K., Lee, J.-B.: Future ozone and  
611 oxidants change under the RCP scenarios, *Atmos. Environ.* 101, 103–115.  
612 <https://doi.org/10.1016/J.ATMOSENV.2014.11.016>, 2015.

613 Kinnison, D. E., Brasseur, G. P., Walters, S., Garcia, R. R., Marsch, D. A., Sassi, F., Boville, B. A.,  
614 Harvey, V. L., Randall, C. E., Emmons, L., Lamarque, J. F., Hess, P., Orlando, J. J., Tie, X. X.,  
615 Randel, W., Pan, L. L., Gettelman, A., Granier, C., Diehl, T., Niemaier, U., and Simmons, A. J.:  
616 Sensitivity of chemical tracers to meteorological parameters in the MOZART-3 chemical transport  
617 model, *J. Geophys. Res.*, 112, D20302, <https://doi.org/10.1029/2006JD007879>, 2007.

618 Kleinman, I., Daum, P. H., Lee, Y.-N., Nunnermacker, L. J., Springston, S. R., Weinstein-Lloyd, J.,  
619 Rudolph, J.: Ozone production efficiency in an urban area, *J. Geophys. Res.*, 107(D23), 4733,  
620 <https://doi.org/10.1029/2002JD002529>, 2002.

621 Koffi, B., Dentener, F., Janssens-Maenhout, G., Guizzardi, D., Crippa, M., Diehl, T., Galmarini, S.,  
622 Solazzo, E.: Hemispheric Transport Air Pollution (HTAP): Specification of the HTAP2 experiments–  
623 Ensuring harmonized modelling, EUR 28255 EN, Luxembourg: Publications Office of the European  
624 Union, <https://doi.org/10.2788/725244>, 2016.

625 Kong, L., Tang, X., Zhu, J., Wang, Z., Li, J., Wu, H., Wu, Q., Chen, H., Zhu, L., Wang, W., Liu, B.,  
626 Wang, Q., Chen, D., Pan, Y., Song, T., Li, F., Zheng, H., Jia, G., Lu, M., Wu, L., and Carmichael, G.  
627 R.: A 6-year-long (2013–2018) high-resolution air quality reanalysis dataset in China based on the

628 assimilation of surface observations from CNEMC, *Earth Syst. Sci. Data*, 13, 529–570,  
629 <https://doi.org/10.5194/essd-13-529-2021>, 2021.

630 Lamarque, J.-F., Emmons, L. K., Hess, P. G., Kinnison, D. E., Tilmes, S., Vitt, F., Heald, C. L., Holland,  
631 E. A., Lauritzen, P. H., Neu, J., Orlando, J. J., Rasch, P. J., and Tyndall, G. K.: CAM-chem:  
632 description and evaluation of interactive atmospheric chemistry in the Community Earth System  
633 Model, *Geosci. Model Dev.*, 5, 369–411, <https://doi.org/10.5194/gmd-5-369-2012>, 2012.

634 Lamarque, J.-F., Shindell, D.T., Josse, B., Young, P.J., Cionni, I., Eyring, V., Bergmann, D., Cameron-  
635 Smith, P., Collins, W.J., Doherty, R., Dalsoren, S., Faluvegi, G., Folberth, G., Ghan, S.J., Horowitz,  
636 L.W., Lee, Y.H., MacKenzie, I.A., Nagashima, T., Naik, V., Plummer, D., Righi, M., Rumbold, S.T.,  
637 Schulz, M., Skeie, R.B., Stevenson, D.S., Strode, S., Sudo, K., Szopa, S., Voulgarakis, A., Zeng, G.:  
638 The Atmospheric Chemistry and Climate Model Intercomparison Project (ACCMIP): overview and  
639 de- scription of models, simulations and climate diagnostics, *Geosci. Model Dev.*, 6, 179–206,  
640 <https://doi.org/10.5194/gmd-6-179-2013>, 2013.

641 Li, J., Nagashima, T., Kong, L., Ge, B., Yamaji, K., Fu, J. S., Wang, X., Fan, Q., Itahashi, S., Lee, H.-J.,  
642 Kim, C.-H., Lin, C.-Y., Zhang, M., Tao, Z., Kajino, M., Liao, H., Li, M., Woo, J.-H., Kurokawa, J.,  
643 Wang, Z., Wu, Q., Akimoto, H., Carmichael, G. R., and Wang, Z.: Model evaluation and  
644 intercomparison of surface-level ozone and relevant species in East Asia in the context of MICS-Asia  
645 Phase III – Part 1: Overview, *Atmos. Chem. Phys.*, 19, 12993–13015, [https://doi.org/10.5194/acp-](https://doi.org/10.5194/acp-19-12993-2019)  
646 [19-12993-2019](https://doi.org/10.5194/acp-19-12993-2019), 2019.

647 Liu, G., Liu, J. J., Tarasick, D. W., Fioletov, V. E., Liu, J., Jin, J., Moeini, O., Sioris, C. E. and Osman,  
648 M.: A global tropospheric ozone climatology from trajectory-mapped ozone soundings, *Atmos. Chem.*  
649 *Phys.* 13, 10659-10675, <https://doi.org/10.5194/acp-13-10659-2013>, 2013.

650 Liu, J., Tarasick, D. W., Fioletov, V. E., McLinden C., Zhao, T., Gong, S., Sioris, C., Jin, J., Liu, G., and  
651 Moeini, O.: A Global Ozone Climatology from Ozone Soundings via Trajectory Mapping: A  
652 Stratospheric Perspective, *Atmos. Chem. Phys.*, 13, 11441-11464, [https://doi.org/10.5194/acp-13-](https://doi.org/10.5194/acp-13-11441-2013)  
653 [11441-2013](https://doi.org/10.5194/acp-13-11441-2013), 2013.

654 Liu, Z., Doherty, R. M., Wild, O., O'Connor, F. M., and Turnock, S. T.: Tropospheric ozone changes and  
655 ozone sensitivity from the present day to the future under shared socio-economic pathways, *Atmos.*  
656 *Chem. Phys.*, 22, 1209–1227, <https://doi.org/10.5194/acp-22-1209-2022>, 2022.

657 Liu, Z., Wild, O., Doherty, R. M., O'Connor, F. M., and Turnock, S. T.: Benefits of Net Zero policies  
658 for future ozone pollution in China, *EGUsphere* [preprint], [https://doi.org/10.5194/egusphere-2023-](https://doi.org/10.5194/egusphere-2023-230)  
659 [230](https://doi.org/10.5194/egusphere-2023-230), 2023.

660 Lu, X., Zhang, L., and Shen, L.: Meteorology and Climate Influences on Tropospheric Ozone: a Review  
661 of Natural Sources, Chemistry, and Transport Patterns, *Current Pollution Reports*, 5, 238–260,  
662 <https://doi.org/10.1007/s40726-019-00118-3>, 2019.

663 Lu, X., Zhang, L., Wang, X., Gao, M., Li, K., Zhang, Y., Yue, X., and Zhang, Y.: Rapid Increases in  
664 Warm-Season Surface Ozone and Resulting Health Impact in China since 2013, *Environ. Sci.*  
665 *Technol. Lett.*, 7, 240–247, <https://doi.org/10.1021/acs.estlett.0c00171>, 2020.

666 Malley, C. S., Henze, D. K., Kuylensstierna, J. C. I., Vallack, H. W., Davila, Y., Anenberg, S. C., Turner,  
667 M. C., Ashmore, M. R.: Updated global estimates of respiratory mortality in adults  $\geq 30$  Years of age  
668 attributable to long-term ozone exposure, *Environ. Health Perspect*, 125, 87021,  
669 <https://doi.org/10.1289/EHP1390>, 2017.

670 Myhre, G., Shindell, D., Breon, F.-M., Collins, W., Fuglestedt, J., Huang, J., Koch, D., Lamarque, J.-  
671 F., Lee, D., Mendoza, B., Nakajima, T., Robock, A., Stephens, G., Takemura, T., Zhang, H.:  
672 Anthropogenic and natural radiative forcing. In: *Climate Change 2013: the Physical Science Basis.*  
673 *Contribution of Working Group I to the Fifth Assessment Report of the Intergovernmental Panel on*  
674 *Climate Change.* Cambridge University Press, Cambridge, United Kingdom and New York, NY,  
675 USA, 659-740, 2013.

676 Neale, R. B., Richter, J., Park, S., Lauritzen, P. H., Vavrus, S. J., Rasch, P. J., and Zhang, M.: The Mean  
677 Climate of the Community Atmosphere Model (CAM4) in forced SST and fully coupled experiments,  
678 *J. Climate*, 26, 5150–5168, <https://doi.org/10.1175/JCLI-D-12-00236.1>, 2013.

679 O'Connor, F. M., Johnson, C. E., Morgenstern, O., Abraham, N. L., Braesicke, P., Dalvi, M., Folberth,  
680 G. A., Sanderson, M. G., Telford, P. J., Voulgarakis, A., Young, P. J., Zeng, G., Collins, W. J., Pyle,  
681 J. A.: Evaluation of the new UKCA climate-composition model – Part 2: the Troposphere, *Geosci.*  
682 *Model Dev.*, 7, 41–91, <https://doi.org/10.5194/gmd-7-41-2014>, 2014.

683 Oleson, K. W., Lawrence, D. M., Bonan, G. B., Flanner, M. G., Kluzek, E., Lawrence, P. J., Levis, S.,  
684 Sean C. Swenson, S. C., Peter, E. T., Dai, A., Decker, M., Dickinson, R., Feddema, J., Heald, C. L.,  
685 Hoffman, F., Lamarque, J.-F., Mahowald, N., Niu, G.-Y., Qian, T., Randerson, J., Running, S.,  
686 Sakaguchi, K., Slater, A., Stöckli, R., Wang, A., Yang, Z. L., Zeng, X.: Technical Description of  
687 version 4.0 of the Community Land Model (CLM) (No. NCAR/TN-478+STR), University  
688 Corporation for Atmospheric Research. <http://dx.doi.org/10.5065/D6FB50WZ>, 2010.

689 O'Neill, B. C., Kriegler, E., Riahi, K., Ebi, K. L., Hallegatte, S., Carter, T. R., Mathur, R., van Vuuren,  
690 D. P.: A new scenario framework for climate change research: the concept of shared socioeconomic  
691 pathways, *Clim. Change*, 122, 387–400, <https://doi.org/10.1007/s10584-013-0905-2>, 2014.

692 Rao, S., Klimont, Z., Smith, S.J., Dingenen, R. Van, Dentener, F., Bouwman, L., Riahi, K., Amann, M.,  
693 Bodirsky, B.L., Van Vuuren, D.P., Reis, L.A., Calvin, K., Drouet, L., Fricko, O., Fujimori, S.,  
694 Gernaat, D., Havlik, P., Harmsen, M., Hasegawa, T., Heyes, C., Hilaire, J., Luderer, G., Masui, T.,  
695 Stehfest, E., Strefler, J., Van Der Sluis, S., Tavoni, M.: Future air pollution in the shared socio-  
696 economic pathways, *Glob. Environ. Chang.*, 42, 346–358,  
697 <https://doi.org/10.1016/j.gloenvcha.2016.05.012>, 2017.



698 Riahi, K., Van Vuuren, D.P., Kriegler, E., Edmonds, J., O'Neill, B.C., Fujimori, S., Bauer, N., Calvin,  
699 K., Dellink, R., Fricko, O., Lutz, W., Popp, A., Cuaresma, J.C., Kc, S., Leimbach, M., Jiang, L., Kram,  
700 T., Rao, S., Emmerling, J., Ebi, K., Hasegawa, T., Havlik, P., Humpenöder, F., Aleluia, L., Silva, D.,  
701 Smith, S., Stehfest, E., Bosetti, V., Eom, J., Gernaat, D., Masui, T., Rogelj, J., Strefler, J., Drouet, L.,  
702 Krey, V., Luderer, G., Harmsen, M., Takahashi, K., Baumstark, L., Doelman, J.C., Kainuma, M.,  
703 Klimont, Z., Marangoni, G., Lotze-Campen, H., Obersteiner, M., Tabeau, A., Tavoni, M.: The Shared  
704 Socioeconomic Pathways and their energy, land use, and greenhouse gas emissions implications: an  
705 overview, *Glob. Environ. Chang.*, 42, 153–168, <https://doi.org/10.1016/j.gloenvcha.2016.05.009>,  
706 2017.

707 Rienecker, M. M., Suarez, M. J., Gelaro, R., Todling, R., Bacmeister, J., Liu, E., Bosilovich, M. G.,  
708 Schubert, S. D., Takacs, L., Kim, G.-K., Bloom, S., Chen, J., Collins, D., Conaty, A., da Silva, A.,  
709 Gu, W., Joiner, J., Koster, R. D., Lucchesi, R., Molod, A., Owens, T., Pawson, S., Pegion, P., Redder,  
710 C. R., Reichle, R., Robertson, F. R., Ruddick, A. G., Sienkiewicz, M., and Woollen, J.: MERRA:  
711 NASA's Modern-Era Retrospective Analysis for Research and Application, *J. Climate*, 24, 3624–  
712 3648, <https://doi.org/10.1175/JCLI-D-11-00015.1>, 2011.

713 Sander, S. P., Friedl, R. R., Barker, J. R., Golden, D. M., Kurylo, M. J., Sciences, G. E., Wine, P. H.,  
714 Abbatt, J. P. D., Burkholder, J. B., Kolb, C. E., Moortgat, G. K., Huie, R. E., and Orkin, V. L.:  
715 Chemical Kinetics and Photochemical Data for Use in Atmospheric Studies Evaluation Number 17  
716 NASA Panel for Data Evaluation, *JLP Publ.*, 10–6, 2011.

717 Shi, X., Zheng, Y., Lei, Y., Xue, W., Yan, G., Liu, X., Cai, B., Tong, D., Wang, J.: Air quality benefits  
718 of achieving carbon neutrality in China, *Sci. Total Environ.*, 795, 148784,  
719 <https://doi.org/10.1016/j.scitotenv.2021.148784>, 2021.

720 Shindell, D. T., Faluvegi, G., Koch, D. M., Schmidt, G. A., Unger, N., and Bauer, S. E.: Improved  
721 Attribution of Climate Forcing to Emissions, *Science*, 326, 716–718,  
722 <https://doi.org/10.1126/science.1174760>, 2009.

723 Stevenson, D. S., Dentener, F. J., Schultz, M. G., Ellingsen, K., van Noije, T. P. C., Wild, O., Zeng, G.,  
724 Amann, M., Atherton, C. S., Bell, N., Bergmann, D. J., Bey, I., Butler, T., Cofala, J., Collins, W. J.,  
725 Derwent, R. G., Doherty, R. M., Drevet, J., Eskes, H. J., Fiore, A. M., Gauss, M., Hauglustaine, D.  
726 A., Horowitz, L. W., Isaksen, I. S. A., Krol, M. C., Lamarque, J.-F., Lawrence, M. G., Montanaro,  
727 V., Müller, J.-F., Pitari, G., Prather, M. J., Pyle, J. A., Rast, S., Rodriguez, J. M., Sanderson, M. G.,  
728 Savage, N. H., Shindell, D. T., Strahan, S. E., Sudo, K., Szopa, S.: Multi-model ensemble simulations  
729 of present-day and near future tropospheric ozone, *J. Geophys. Res.*, 111, D08301,  
730 <https://doi.org/10.1029/2005JD006338>, 2006.

731 Stevenson, D. S., Young, P. J., Naik, V., Lamarque, J.-F., Shindell, D. T., Voulgarakis, A., Skeie, R. B.,  
732 Dalsoren, S. B., Myhre, G., Berntsen, T. K., Folberth, G. A., Rumbold, S. T., Collins, W. J.,  
733 MacKenzie, I. A., Doherty, R. M., Zeng, G., van Noije, T. P. C., Strunk, A., Bergmann, D., Cameron-  
734 Smith, P., Plummer, D. A., Strode, S. A., Horowitz, L., Lee, Y. H., Szopa, S., Sudo, K., Nagashima,

735 T., Josse, B., Cionni, I., Righi, M., Eyring, V., Conley, A., Bowman, K. W., Wild, O., Archibald, A.:  
736 Tropospheric ozone changes, radiative forcing and attribution to emissions in the atmospheric  
737 chemistry and climate model Intercomparison project (ACCMIP), *Atmos. Chem. Phys.* 13, 3063–  
738 3085. <https://doi.org/10.5194/acp-13-3063-2013>, 2013.

739 Sudo, K., Takahashi, M., and Akimoto, H.: Future changes in stratosphere-troposphere exchange and  
740 their impacts on future tropospheric ozone simulations, *Geophys. Res. Lett.*, 30(24), 2256,  
741 <https://doi.org/10.1029/2003GL018526>, 2003.

742 Tang, X., Zhu, J., Wang, Z. F., and Gbaguidi, A.: Improvement of ozone forecast over Beijing based on  
743 ensemble Kalman filter with simultaneous adjustment of initial conditions and emissions, *Atmos.*  
744 *Chem. Phys.*, 11, 12901–12916, <https://doi.org/10.5194/acp-11-12901-2011>, 2011.

745 Tang, X., Kong, L., Zhu, J., Wang, Z. F., Li, J. J., Wu, H. J., Wu, Q. Z., Chen, H. S., Zhu, L. L., Wang,  
746 W., Liu, B., Wang, Q., Chen D. H., Pan Y. P., Song, T., Li, F., Zheng, H. T., Jia, G. L., Lu, M. M.,  
747 Wu, L., and Carmichael, G. R.: A Six-year long High-resolution Air Quality Reanalysis Dataset over  
748 China from 2013 to 2018, V2, *Sci. Data Bank*, <https://doi.org/10.11922/sciencedb.00053>, 2020a.

749 Tang, X., Kong, L., Zhu, J., Wang, Z. F., Li, J. J., Wu, H. J., Wu, Q. Z., Chen, H. S., Zhu, L. L., Wang,  
750 W., Liu, B., Wang, Q., Chen D. H., Pan Y. P., Song, T., Li, F., Zheng, H. T., Jia, G. L., Lu, M. M.,  
751 Wu, L., and Carmichael, G. R.: A Six-year long High-resolution Air Quality Reanalysis Dataset over  
752 China from 2013 to 2018 (monthly and annual version), V1, *Sci. Data Bank*,  
753 <https://doi.org/10.11922/sciencedb.00092>, 2020b.

754 Tie, X., Madronich, S., Walters, S., Edwards, D. P., Ginoux, P., Mahowald, N., Zhang, R. Y., Lou, C.,  
755 Brasseur, G.: Assessment of the global impact of aerosols on tropospheric oxidants, *J. Geophys. Res.*,  
756 110, D03204, <https://doi.org/10.1029/2004JD005359>, 2005.

757 Tilmes, S., Lamarque, J.-F., Emmons, L. K., Kinnison, D. E., Ma, P.-L., Liu, X., Ghan, S., Bardeen, C.,  
758 Arnold, S., Deeter, M., Vitt, F., Ryerson, T., Elkins, J. W., Moore, F., Spackman, J. R., and Val  
759 Martin, M.: Description and evaluation of tropospheric chemistry and aerosols in the Community  
760 Earth System Model (CESM1.2), *Geosci. Model Dev.*, 8, 1395–1426, <https://doi.org/10.5194/gmd-8-1395-2015>, 2015.

762 Tong, D., Cheng, J., Liu, Y., Yu, S., Yan, L., Hong, C., Qin, Y., Zhao, H., Zheng, Y., Geng, G., Li, M.,  
763 Liu, F., Zhang, Y., Zheng, B., Clarke, L., and Zhang, Q.: Dynamic projection of anthropogenic  
764 emissions in China: methodology and 2015–2050 emission pathways under a range of socio-  
765 economic, climate policy, and pollution control scenarios, *Atmos. Chem. Phys.*, 20, 5729–5757,  
766 <https://doi.org/10.5194/acp-20-5729-2020>, 2020.

767 Turnock, S. T., Wild, O., Sellara, A., O'Connor, F. M.: 300 years of tropospheric ozone changes using  
768 CMIP6 scenarios with a parameterised approach. *Atmos. Environ.*, 213, 686–698,  
769 <https://doi.org/10.1016/j.atmosenv.2019.07.001>, 2019.

770 Turnock, S. T., Wild, O., Dentener, F. J., Davila, Y., Emmons, L. K., Flemming, J., Folberth, G. A.,  
771 Henze, D. K., Jonson, J. E., Keating, T. J., Kengo, S., Lin, M., Lund, M., Tilmes, S., O'Connor, F.  
772 M.: The impact of future emission policies on tropospheric ozone using a parameterised approach,  
773 *Atmos. Chem. Phys.*, 18, 8953–8978, <https://doi.org/10.5194/acp-18-8953-2018>, 2018.

774 Voulgarakis, A., Naik, V., Lamarque, J.-F., Shindell, D. T., Young, P. J., Prather, M. J., Wild, O., Field,  
775 R. D., Bergmann, D., CameronSmith, P., Cionni, I., Collins, W. J., Dalsøren, S. B., Doherty, R. M.,  
776 Eyring, V., Faluvegi, G., Folberth, G. A., Horowitz, L. W., Josse, B., MacKenzie, I. A., Nagashima,  
777 T., Plummer, D. A., Righi, M., Rumbold, S. T., Stevenson, D. S., Strode, S. A., Sudo, K., Szopa, S.,  
778 and Zeng, G.: Analysis of present day and future OH and methane lifetime in the ACCMIP  
779 simulations, *Atmos. Chem. Phys.*, 13, 2563–2587, <https://doi.org/10.5194/acp-13-2563-2013>, 2013.

780 Wang, Y., Liao, H.: The impacts of transport from South and Southeast Asia on O<sub>3</sub> concentrations in  
781 China from 2015 to 2050, *Chinese Science Bulletin (in Chinese)*, 67(18), 2043-2059,  
782 <https://doi.org/10.1360/tb-2021-0707>, 2022.

783 Wang Y., Shen, L., Wu, S., Mickley, L., He, J., Hao, J.: Sensitivity of surface ozone over China to 2000–  
784 2050 global changes of climate and emissions, *Atmos. Environ.*, 75, 374-382,  
785 <https://doi.org/10.1016/j.atmosenv.2013.04.045>, 2013.

786 Wang, T., Wei, X. L., Ding, A. J., Poon, C. N., Lam, K. S., Li, Y. S., Chan, L. Y., and Anson, M.:  
787 Increasing surface ozone concentrations in the background atmosphere of Southern China, 1994–  
788 2007, *Atmos. Chem. Phys.*, 9, 6217–6227, <https://doi.org/10.5194/acp-9-6217-2009>, 2009.

789 Wang, Z. F., Sha, W. M., and Ueda, H.: Numerical modeling of pollutant transport and chemistry during  
790 a high-ozone event in northern Taiwan, *Tellus B*, 52, 1189–1205, <https://doi.org/10.1034/j.1600-0889.2000.01064.x>, 2000.

792 Wild, O.: Modelling the global tropospheric ozone budget: exploring the variability in current models,  
793 *Atmos. Chem. Phys.*, 7, 2643–2660, <https://doi.org/10.5194/acp-7-2643-2007>, 2007.

794 Wild, O. and Akimoto, H.: Intercontinental transport of ozone and its precursors in a three-dimensional  
795 global CTM, *J. Geophys. Res.*, 106(D21), 27729–27744, <https://doi.org/10.1029/2000jd000123>, 2001.

796 Wild, O., Fiore, A. M., Shindell, D. T., Doherty, R. M., Collins, W. J., Dentener, F. J., Schultz, M. G.,  
797 Gong, S., MacKenzie, I. A., Zeng, G., Hess, P., Duncan, B. N., Bergmann, D. J., Szopa, S., Jonson,  
798 J. E., Keating, T. J., and Zuber, A.: Modelling future changes in surface ozone: a parameterized  
799 approach, *Atmos. Chem. Phys.*, 12, 2037–2054, <https://doi.org/10.5194/acp-12-2037-2012>, 2012.

800 Xu, B., Wang, T., Ma, D., Song, R., Zhang, M., Gao, L., Li, S., Zhuang, B., Li, M., Xie, M.: Impacts of  
801 regional emission reduction and global climate change on air quality and temperature to attain carbon  
802 neutrality in China, *Atmos. Res.*, <https://doi.org/10.1016/j.atmosres.2022.106384>, 2022.

803 Yang, X. L., Zhou, B. T., Xu, Y., and Han, Z.-Y.: CMIP6 Evaluation and Projection of Temperature and  
804 Precipitation over China, *Adv. Atmos. Sci.*, 38(5), 817–830, [https://doi.org/10.1007/s00376-021-](https://doi.org/10.1007/s00376-021-0351-4)  
805 0351-4, 2021.

806 Young, P. J., Archibald, A. T., Bowman, K. W., Lamarque, J.-F., Naik, V., Stevenson, D. S., Tilmes, S.,  
807 Voulgarakis, A., Wild, O., Bergmann, D., Cameron-Smith, P., Cionni, I., Collins, W. J., Dalsøren, S.  
808 B., Doherty, R. M., Eyring, V., Faluvegi, G., Horowitz, L. W., Josse, B., Lee, Y. H., MacKenzie, I.  
809 A., Nagashima, T., Plummer, D. A., Righi, M., Rumbold, S. T., Skeie, R. B., Shindell, D. T., Strode,  
810 S. A., Sudo, K., Szopa, S., and Zeng, G.: Pre-industrial to end 21st century projections of tropospheric  
811 ozone from the Atmospheric Chemistry and Climate Model Intercomparison Project (ACCMIP),  
812 *Atmos. Chem. Phys.*, 13, 2063–2090, <https://doi.org/10.5194/acp-13-2063-2013>, 2013.

813 Young, P. J., Naik, V., Fiore, A. M., Gaudel, A., Guo, J., Lin, M. Y., Neu, J. L., Parrish, D. D., Rieder,  
814 H. E., Schnell, J. L., Tilmes, S., Wild, O., Zhang, L., Ziemke, J., Brandt, J., Delcloo, A., Doherty, R.  
815 M., Geels, C., Hegglin, M. I., Hu, L., Im, U., Kumar, R., Luhar, A., Murray, L., Plummer, D.,  
816 Rodriguez, J., Saiz-Lopez, A., Schultz, M. G., Woodhouse, M. T., Zeng, G.: Tropospheric Ozone  
817 Assessment Report: Assessment of global-scale model performance for global and regional ozone  
818 distributions, variability, and trends, *Elem. Sci. Anth.*, 6, 10, <https://doi.org/10.1525/elementa.265>,  
819 2018.

820 Zanis, P., Akritidis, D., Turnock, S., Naik, V., Szopa, S., Georgoulias, A. K., Bauer, S. E., Deushi, M.,  
821 Horowitz, L. W., Keeble, J., Sager, P. L., O'Connor, F. M., Oshima, Naga., Tsigaridis, K. and Noije,  
822 T.: Climate change penalty and benefit on surface ozone: A global perspective based on CMIP6 Earth  
823 system models, *Environ. Res. Lett.*, 17, 024014, <https://doi.org/10.1088/1748-9326/ac4a34>, 2022.

824 Zaveri, R. A., Berkowitz, C. M., Kleinman, L. I., Springston, S. R., Doskey, P. V., Lonneman, W. A.,  
825 Spicer, C. W.: Ozone production efficiency and NO<sub>x</sub> depletion in an urban plume: Interpretation of  
826 field observations and implications for evaluating O<sub>3</sub>-NO<sub>x</sub>-VOC sensitivity, *J. Geophys. Res.*,  
827 108(D14), 4436, <https://doi.org/10.1029/2002JD003144>, 2003.

828 Ziemke, J. R., Chandra, S., Labow, G. J., Bhartia, P. K., Froidevaux, L., and Witte, J. C.: A global  
829 climatology of tropospheric and stratospheric ozone derived from Aura OMI and MLS measurements,  
830 *Atmos. Chem. Phys.*, 11, 9237–9251, <https://doi.org/10.5194/acp-11-9237-2011>, 2011.

831 Zhu, J. and Liao, H.: Future ozone air quality and radiative forcing over China owing to future changes  
832 in emissions under the Representative Concentration Pathways (RCPs), *J. Geophys. Res.: Atmos.*,  
833 121, 1978 – 2001, <https://doi.org/10.1002/2015JD023926>, 2016.